Probabilistic Assessment of the Impact of Integrating Large-Scale High-Power Fast Charging Stations on the Power Quality in the Electric Power Distribution Systems

by

Bishoy Basta

A thesis submitted to the
School of Graduate and Postdoctoral Studies in partial
fulfillment of the requirements for the degree of

Master of Applied Science

Faculty of Engineering and Applied Science

In The Department of Electrical, Computer and Software Engineering

University of Ontario Institute of Technology (Ontario Tech University)

Oshawa, Ontario, Canada

Mar. 2020

THESIS EXAMINATION INFORMATION

Submitted by: **Bishoy Basta**

Mater of Applied Science in **Electrical and Computer Engineering**

Thesis title: Probabilistic Assessment of the Impact of Integrating Large-Scale High-Power Fast Charging Stations on the Power Quality in the Electric Power Distribution Systems

An oral defense of this thesis took place on March 20, 2020 in front of the following examining committee:

Examining Committee:

Chair of Examining Committee	Dr. Ying Wang
Research Supervisor	Dr. Walid Morsi Ibrahim
Examining Committee Member	Dr. Sheldon Williamson
Examining Committee Member	Dr. Khalid Elgazzar
Thesis Examiner	Dr. Haoxiang Lang
External Examiner	Dr. Haoxiang Lang

The above committee determined that the thesis is acceptable in form and content and that a satisfactory knowledge of the field covered by the thesis was demonstrated by the candidate during an oral examination. A signed copy of the Certificate of Approval is available from the School of Graduate and Postdoctoral Studies.

ABSTRACT

The work presented in this thesis assesses the impacts of integrating large-scale high-power fast charging stations on the electric power quality by studying different power quality phenomena such as low-order and high-order harmonics, supraharmonics and voltage/light flickering. New three-phase effective power quantities are developed at both the low-order (harmonics below 40th order) and high order (harmonics above 40th order) and are used to quantify such harmonic impact. Chargers from two different manufacturers are used in this study and the real measurement are performed at fast charging stations in Canada. The Monte Carlo method is used to probabilistically estimate the electrical vehicles (EV) power demand when charging from the fast charging stations. The IEEE 34-bus standard test distribution system is employed to simulate the different impacts from different chargers' manufactures. The results have shown that the chargers from different manufacturers may contribute differently in terms of the harmonic distortion levels reaching 18% at the system level. Furthermore, the frequency spectrum of the chargers from different manufacturers are different at both the low-order and high-order harmonics. The results have also shown that the new three-phase power quantities defined in this work are useful in identifying the chargers with high contribution to both the low-order and the high-order harmonics distortion/interference by separating the power quantities defined in the IEEE Standard 1459-2010 into several power quantities at the low-order harmonic (ranging from 2nd to 39th harmonic order or below 2.4 kHz) and the high-order harmonics (beyond 40th harmonic order or beyond 2.4 kHz).

Keywords: Fast charging stations; harmonics; plug-in electric vehicles; power quantities; Supraharmonics.

AUTHOR'S DECLARATION

I hereby declare that this thesis consists of original work of which I have authored. This is a true copy of the thesis, including any required final revisions, as accepted by my examiners.

I authorize the University of Ontario Institute of Technology (Ontario Tech University) to lend this thesis to other institutions or individuals for the purpose of scholarly research. I further authorize University of Ontario Institute of Technology (Ontario Tech University) to reproduce this thesis by photocopying or by other means, in total or in part, at the request of other institutions or individuals for the purpose of scholarly research. I understand that my thesis will be made electronically available to the public.

Bishoy Basta

STATEMENT OF CONTRIBUTIONS

Published Work

S. A. El-Battawy ; B. Basta ; W. G. Morsi “Impact of Integrating Electric Vehicles and Rooftop Solar Photovoltaic on Transformer's Aging Considering the Effect of Ambient Temperature” 2018 IEEE Electrical Power and Energy Conference (EPEC), 2018

Part of the work described in Chapter 3 has been Submitted to be published as:

B. Basta, W. G. Morsi, “Low and High Order Harmonic Distortion in the Presence of Fast Charging Stations,” Electric Power Systems Research (EPSR), 2019. Under Review

ACKNOWLEDGEMENTS

I would like to acknowledge with great emphasis the contributions of my supervisor Dr. Walid Morsi Ibrahim, for all the late nights and great amount of effort that has gone into supporting my work. It is his attention to detail and determination that has motivated me to go further than I would have thought possible. He supported me from day one in the research field and always encourage me especially in some down moments when I feel it's impossible to do it.

I would also like to thank Faculty of Engineering and Applied Science (FEAS) and The Power Workers' Union Transportation Electrification and Smart Grid Research for supporting scholarship award that I received for supporting my work.

TABLE OF CONTENTS

LIST OF TABLES

CHAPTER 2

CHAPTER 3

CHAPTER 4

CHAPTER 5

CHAPTER 6

LIST OF FIGURES

CHAPTER 2

CHAPTER 3

CHAPTER 4

CHAPTER 5

CHAPTER 6

LIST OF ABBREVIATIONS AND SYMBOLS

ANSI	American National Standards Institute
IEEE	The Institute of Electrical and Electronics Engineers
MCS	Monte Carlo Simulation
PEV	Plug-in Electric Vehicle
SOC	State of Charge
SOC_{min}	Minimum State of Charge
AC	alternating current
FCS	fast charging station
EVs	electrical vehicles
THDv	Total Harmonic Voltage Distortion
THD_{eI}	Equivalent total harmonic distortion
PCC	Point of Common Coupling
ISC/IL	short circuit current to the maximum load current
P_{ST}	short-term perception of flicker
P_{LT}	long-term perception of flicker
LV	Low voltage
MV	Medium voltage
S_{eN}	non-fundamental effective apparent power
S_{eNL}	low order harmonic effective non-fundamental apparent power
S_{eNH}	high order harmonic effective non-fundamental apparent power
S_{eNI}	harmonic interference effective non-fundamental apparent power
rms	root mean square
V_{e1}	fundamental effective voltage
I_{e1}	fundamental effective current
D_{eI}	effective current distortion power

HPF	the harmonic pollution factor
she	effective harmonic apparent power
BESS	battery energy storage system
TFWG	Test Feeder Working Group

Chapter 1. Introduction

1.1 Background

Increasing the number of fast charging stations (FCS) became the target of many Canadian jurisdictions to increase the adoption of electrical vehicles (EVs), making longer drives possible for different models of EVs. According to a new report compiled by British financial services firm [1] there are 23,620 electrical vehicle and only 5,841 charging stations across Canada. New entrants like Petro-Canada and Electrify Canada are working to add dozens of fast-chargers across the country this year, meanwhile Petro-Canada announced that it would add 50 fast-charging stations across the Trans-Canada Highway, as per Global news report on Feb. 2019 [2], [3]. The integration of large-scale high-power fast charging stations (or level three chargers) will eventually reduce the charging time of the plug-in electric vehicles (PEVs) as well as will facilitate the adoption of on the road charging. The chargers, generally with a capacity of 50 kilowatts, can provide an electric driving range of nearly 320 kilometers for a single charge of one hour, far faster than the overnight charging of 6.6-kilowatt level two chargers that owners can install in their homes [4], which typically takes 3.5 hours. In the past few years, several automakers have been working on increasing the electric driving range of the plug-in electric vehicles (PEVs) to address the customers' concerns regarding the limited electric driving range of PEVs. As a result, the home charging becomes very challenging since it results into a very prolonged charging time, which has not been well received by the public. In order to address this challenge, several automakers and many Canadian jurisdictions have started to build high-power fast charging stations (FCS) that are considered level 3 chargers (e.g. rated 50 kW [5]) to reduce the charging time[6]–[8] .

1.2 Statement of the Problem

Increasing the penetration of FCSs means increasing the high-power loads in the primary distribution system, which may affect the power quality of the electrical power in the distribution systems. Low order harmonics (below 2kHz), harmonics distortion in the frequency range 2 to 150 kHz, referred to as supraharmonics [9], voltage flickers etc., are examples of the distortion that caused by nonlinear loads such as the FCS.

Traditionally, most of the non-linear loads that used to exist on the power system before contribute with harmonic distortion in the low order frequency only following the equations and limits in IEEE 519- 2014 [10]. Besides, most of the literatures investigate the study of harmonic distortion at low frequency range.

The electric power distribution grid typically consists of a primary and a secondary system. The primary system is the upper hierarchical level, which connects with the transmission system represented by the distribution substation and delivers power to the secondary system throughout its distribution feeders. The primary system also includes various regulating devices including but not limited to capacitor banks and load tap changing transformers. The main functions of these regulating devices are to improve the voltage profile and reduce the distribution system losses. The fast charging stations are typically supplied from the three-phase primary distribution systems. The integration of the fast charging stations imposes an additional burden on the electric power grid, as the high charging loads of fast EV charging stations will degrade the power quality of the distribution network. The poor voltage profile, the increased power demand and the harmonic distortions are some of the consequences of the uncoordinated charging of

PEVs. Thus, the impact of increasing the penetration of the high-power fast charging stations on the existing strained distribution system need more investigation.

The voltage quality and the power quality need to be assessed considering the impact of such large scale of high-power fast charging stations so the electric utilities will have an idea about the impact of increasing the numbers of the fast charging stations in the primary system so to prevent customers from experiencing poor power quality and interruptions. Furthermore, there are currently different manufacturers of high-power fast chargers that are used in fast charging stations. The harmonic distortion emission from these fast chargers needs careful investigation and through assessment to understand the negative impacts at both the fast charging station level and at the distribution system level.

The work presented in this thesis focuses on quantifying the impacts of increasing the penetration of high-power fast charging stations on the electric power quality using novel power quantities that are developed in this work. These novel power quantities will be applied in comparison with standards regulating distribution system operation and will be used to define limits on the respective power quality indices. Using these new power quantities will help to investigate and compare between the impact of integrating large-scale of high-power fast charging station from different manufacturer in terms of low order harmonic distortion, high order harmonic distortion and interference power between the low and high current/ voltage distortions. The power quality assessment includes harmonics, supraharmonics, voltage and light flickers, which will be quantified by performing a Monte Carlo simulation to address the probabilistic nature of PEV

charging in FCS. Finally, the results are presented which takes into consideration the effect of FCS chargers from different manufacturers and also different PEVs make.

1.3 Thesis Objectives and Contributions.

The following represents the research objectives of the work presented in this thesis.

- Studying the charging profiles of PEVs when charging at high-power fast charging stations considering different chargers from different manufacturers and different PEV types using real-measurements.
- Modeling the FCS charging profile considering chargers from different manufacturers and different PEVs types on the system level, in order to study the harmonic propagation in low and high order harmonic distortion range.
- Studying the effect of integrating high-power fast charging stations on the electric power quality at both the FCS level and at the system level.
- Developing new power quantities to separate the low-order harmonics (ranging from 2^{nd} to 39^{th} harmonic order or below 2.4 kHz) and the high-order harmonics (beyond 40^{th} harmonic order or beyond 2.4 kHz).
- Study and compare the current/voltage distortion between different manufacturers in terms of low order distortion, high order distortion at system level.
- Apply the new developed power quantities to compare between the manufacturers for low order distortion power, high order distortion power and interference power resulting from low and high order current/voltage distortions.
- Investigate the effect of the voltage fluctuations and light flickers on the power distribution system in presence of the fast charging stations at the system level.

1.4 Thesis Organization

The work of this thesis is organized as follows:

Chapter 2 surveys the previous work investigating the impact of fast charging stations on the electric distribution system. This review will give an insight on how previous work has addressed the problem from a system impact analysis perspective, including the analysis methods used as well as notable areas which can be improved upon for a more detailed investigation.

Chapter 3 summarizes the aspects of fast charging stations impacts on the distribution system that are relevant to the power quality phenomena. Specifically, harmonics, supra-harmonics and voltage fluctuations and the appropriate mathematical formulations of the power quantities in light of the IEEE standard 1549-2010 are presented. The chapter also sheds light on the relevant power quality standards (ANSI-C84.1-2011 and EN50160) and the recommended limits with respect to these power quality phenomena in the IEEE 519-2014.

Chapter 4 describes field measurements that have been done including three types of electrical vehicles and two different types of fast chargers from different manufacturers. This chapter also shows the impact of PEV charging at the FCS level with different aspects and compare the results with the specified limits in the standards.

Chapter 5 describes the modeling of the electric primary distribution system components, including the primary system circuits, the spot loads and the FCSs loads, which consists of twenty fast charging stations. This chapter also presents the use of the Monte Carlo method to probabilistically estimate the fast charging stations loads, and the MC convergence.

Chapter 6 presents the results of implementing the proposed approach to incorporate the fast charging stations load to the IEEE 34-bus standard test system using a Monte Carlo simulation after modifying it to estimate the charging profile of the FCSs. The probabilistic assessment of the electric power quality considering different vehicle types, and chargers' types and vehicle penetration are presented. Finally, the conclusions are presented in Chapter 7

Chapter 2. Literature review

2.1 Introduction

The literature review in this section is intended to review the previous work investigating the impact of the electrical vehicles fast charging stations on the electrical power quality in the electric primary distribution systems. The work of the electrical vehicle charger is divided into two main sections, level one and level two chargers, which charging the PEVs from low voltage supply at the secondary distribution system (120V and 240V respectively), and level three (or DC charger), which named as fast (ultra-fast) charging station, and its characteristically as high-power stations and are connected to the primary distribution system with MV supply. This study focusses on the level three chargers and its impact on the primary distribution system.

On the other hand, most of the previous work focuses on assessing the voltage quality in terms of voltage fluctuations, and voltage magnitude deviations, some studies concentrated on the power quality in terms of harmonics orders in low-order and high-order harmonics. Different rated fast charging stations power are considered in previous work with different impacts on the power quality. The aim of this chapter is to review the previous work that has been done on fast charging stations impact on power quality in terms of harmonics and voltage fluctuations.

2.2 Voltage fluctuation and limits:

The study in [11], investigated the power quality impacts of the FCSs (Fast Charging Stations) in terms of voltage fluctuations. It includes different ratings of FCS, 60 kW, 150 kW, 240 kW and 350 kW. To conclude the finding, there are no voltage variation

violating the IEEE standard limits in 60 kW FCS, while in case of 150 kW, 240 kW and 350 kW the voltage violates the borderline of irritation.

The study indicated that because of the grid stiffness surrounding the analyzed fast charging station, the large power drawn did not significantly affect the power quality. However, in some distant charger locations e.g. on highways, it should be considered that the electrical power grid might be noticeably weaker. In such a case the high-power DC charging stations may affect the quality of supply.

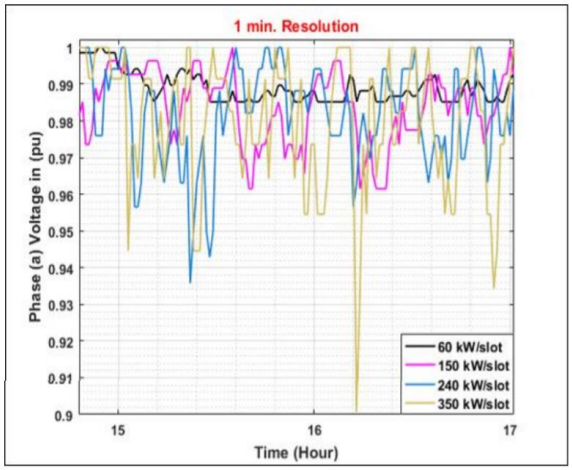

Figure 2.1: Effect of increasing the rated power of the FCS on the bus voltage.

2.3 Harmonics analysis:

the study in [12] looked at the impact of low-order harmonic emission from fast charging stations. The study reported that some individual low-order harmonics in particular the11^{th} and the 13^{th} failed to comply with both standards IEEE 519 [10] and IEC 61000-3-12/2-4 [13], [14], (5% and 3% respectively) .

Supraharmonics, which is defined as the harmonics distortion in the band of 2 kHz to 150 kHz, are studied in [15], [16]and [17]. These studies considered the supraharmonics

distortion with DC fast charging stations using models to simulate the accurate impact of using inverters AC/DC on supraharmonics emission. The main findings of these studies are the electrical vehicle fast chargers emit harmonics in the high frequency range, which is called supraharmonics and it propagates in the distribution system, but the studies concluded that there still remains a lack of knowledge that prevents the understanding of the origin and the spread of supraharmonics. Such knowledge is required to avoid future interference, but also to avoid the setting of unnecessary strict requirements on end-user equipment or on network operators.

The work in [18] highlighted the impact of the fast charging stations in terms of low-order harmonic emission. The study indicates the general structure diagram of high-power DC charger Figure 2.2.

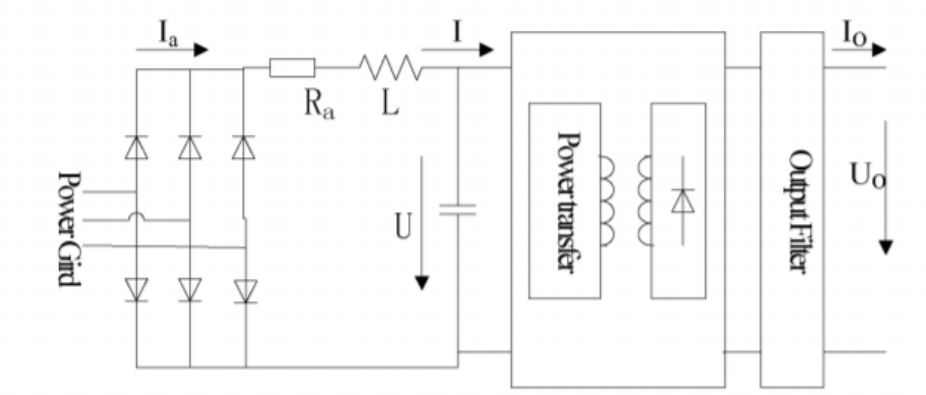

Figure 2.2: Topologic Structure Diagram of DC Charger.

The study anticipated the simultaneous charging of PEVs through fast charging stations to cause high harmonic pollution to the distribution networks, which may reach 24%.

The work in [19], [20] investigated the risk of harmonic resonance in the Dutch MV grid in the presence of fast charging stations. The study found a resonance peaked at 1.25 kHz as in Figure 2.3 and hence it was concluded that such resonance should be

considered by the distribution network operators when it comes to large-scale integration of fast charging stations.

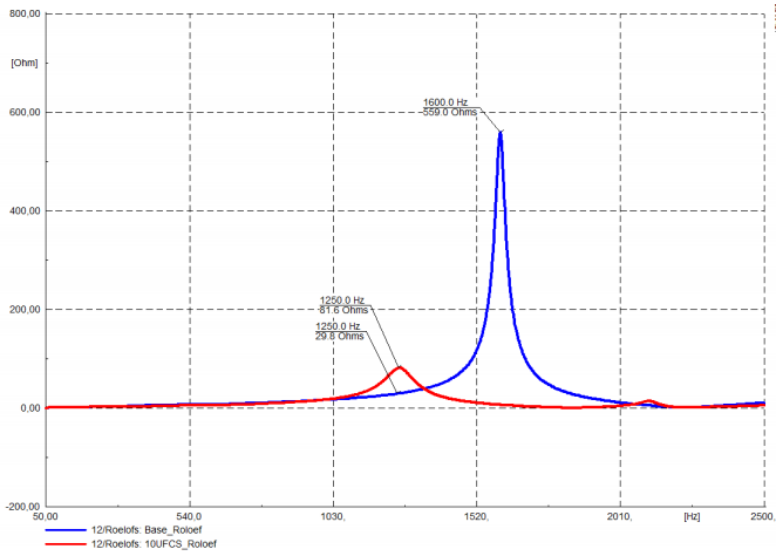

Figure 2.3: Frequency sweep results at MV bus 12 with and without ultra-fast charging station connections.

The study in [21] looked into the low-order harmonic characteristics of electric vehicles in fast charging stations. It includes measurements at the fast charging stations level and at the simulation level. Different electrical vehicles with different battery capacity are used in the measurements. The IEEE 14 nodes test distribution feeder system is used to simulate the harmonic effect of fast charging stations on the test system. The study reported low-order harmonic distortion in the current ranging from 8% and up to 19%. The study also reported that the low-order harmonic distortion exceeded the distortion limit, which is 5%.

The work in [22] reported a total harmonic distortion in the current from fast charging stations reaching 26.92% with increasing the number of charging vehicles in fast charging stations using 24-hour simulation with probability distribution demand for the

fast charging stations as shown in figure 2.4, while the study didn't report any harmonics distortion bigger than 8th harmonic order.

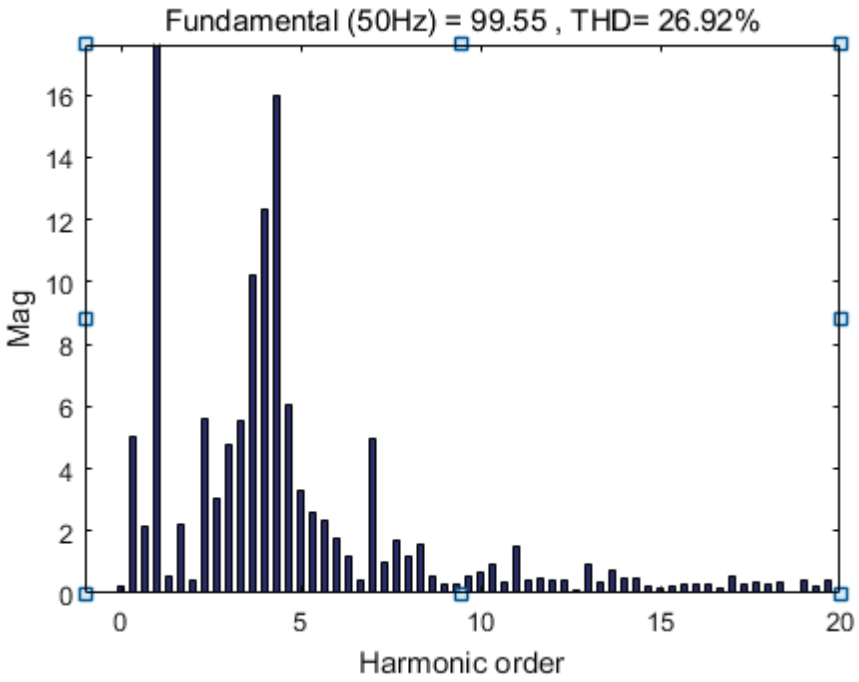

Figure 2.4: Harmonic analysis for three chargers working together

The work in [23] presented a study of the load profile and harmonic impact of a charging station on the medium voltage in a distribution system in Chiang Mai (Thailand). The study used the load profile of the substation in winter and summer as in Figure 2.5. The percentages of THD_v profiles of the substation were similar in both summer and winter, with high values during light loads at 3 to 9 a.m., and low values when the peak load was in the daytime and evening as in Figure 2.6. The harmonic current pattern of a 50 kW DC charger is shown in Figure 2.7 and the dominants harmonic order in the current are the 5th, 11th, 13th, 17th and 19th.

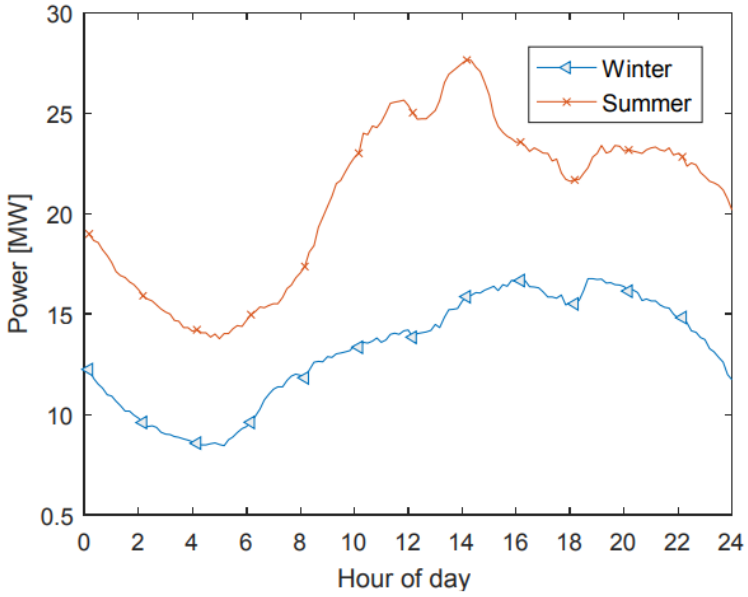

Figure 2.5: Total harmonic distortion of voltage (%THDv) profile of substation

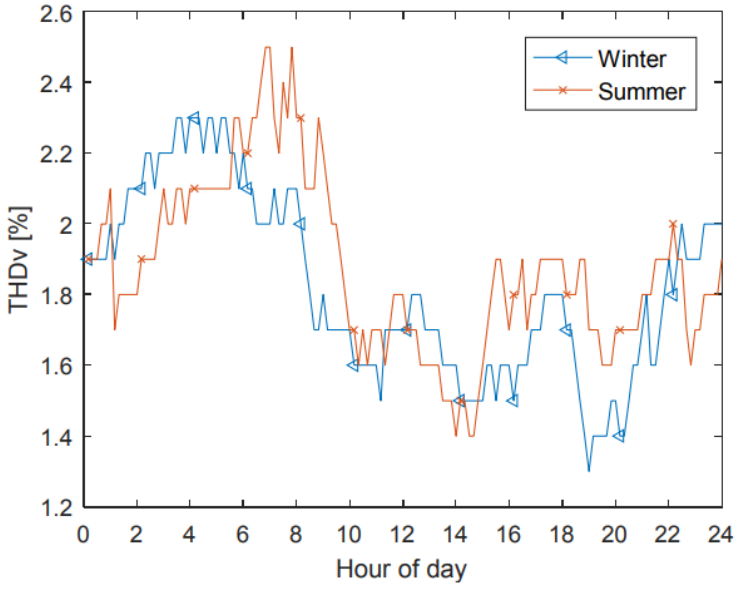

Figure 2.6: Substation Load Profile in Summer and Winter

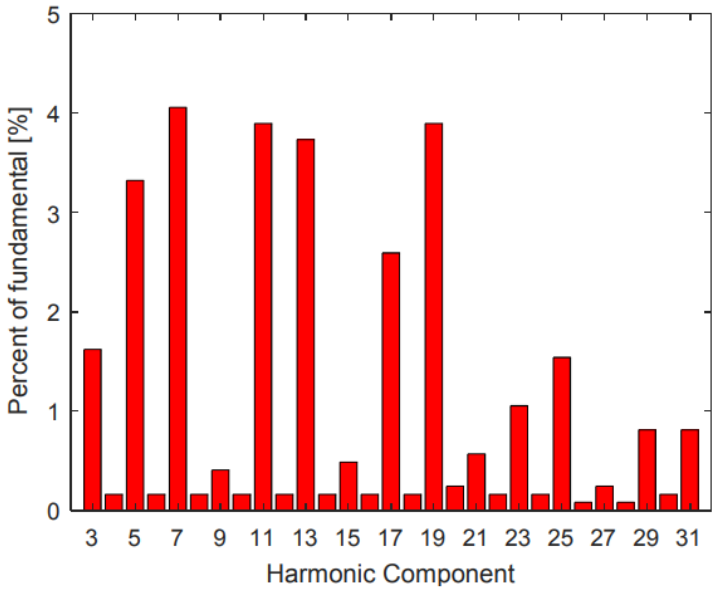

Figure 2.7: Current harmonics of DC charging

The results show that the load profile during the peak load during the summer retains the original shape in case without the charging station load. However, between 9 to 10 a.m. the increase in the load demand was noticeable. The peak $\%THD_v$ of 50% EV charging penetration is 4.04% and occurred from 9 a.m. to 10 a.m.

The study in [24] discussed the impact of harmonics due to fast charging stations and it concluded that the high-order harmonics may become problematic to the distribution system. The study in [25] looked into the harmonic emission resulted from charging PEV in fast charging stations and it reported considerable harmonic current emission at the 3^{rd}, 5^{th} and 7^{th} low-order harmonics and as well as a significant high-order harmonic (supraharmonics).

Table 2.1 Overview of previous studies on Fast Charging Stations

Paper Reference	Time resolution	Voltage fluctuation	Harmonics	Supraharmonics	Comparison to standards
[11]	1 min	√	x	x	√
[12]	x	x	√	x	x
[16], [17]	x	x	x	√	x
[18]	Daily	√	x	x	x
[19], [20]	x	x	√	x	x
[21]	x	x	√	x	√
[22]	hourly	x	√	x	x
[23]	x	x	√	√	x
[24]	x	x	√	√	√
[25]	x	x	√	√	√

The work presented in this thesis aimed to address the impact of increasing the penetration of the fast charging stations on the electric power quality in the electric distribution system. Specifically, this thesis presents a simulation using IEEE 34 Bus standard test feeder to help assessing the impact at the system level. The study also includes different vehicle types and different charger manufacturers while considering different electrical vehicles penetration.

2.4 Summary:

This Chapter surveys the previous work published in the literature investigating the impact of fast charging stations on the electric power distribution system. This review will give an insight on how previous work has addressed the problem from a system impact analysis perspective, including the analysis methods used as well as notable areas, which can be improved upon for a more detailed investigation.

Chapter 3. Aspects of fast charging stations impacts on the distribution systems: Harmonics, Supra-harmonics and voltage fluctuations

3.1 Introduction

The concept of transportation electrification is gaining so much attention in the past few years. Electric vehicle (EV) production has grown 10 times over the past four years and EV sales will grow 14 times over the next ten years [26]. DC fast charging can deliver 100 RPH (Miles of Range per Hour of Charging) or more, charging some EVs to 80 percent in 20-30 minutes. DC fast charging stations have various power levels. In general, higher power levels charge EVs faster [26]. Fast charging aims to recharge EV batteries within a short period similar to that for gasoline refueling of conventional vehicles. Thus, the total travelling distance of EVs can be greatly extended. Although fast charging enables EVs to have a driving range like that of conventional vehicles, it may have adverse impacts on the electric power distribution system, in particular power quality in the form of harmonics, supra-harmonics and voltage fluctuation. This may affect the entire power distribution system due to the propagation of the harmonics and supra-harmonics in the system [15].

The FCSs are utilized to recharge such PEVs but need to be supplied with high power to reduce the charging time of PEVs. From the perspective of stakeholders, FCSs are intended to meet various objectives such as reducing the charging and the waiting time of the PEVs, supporting long-distance trip, and thus the public may be able to rely more on such technology and then adopts it [27]. From the distribution systems perspective, the PEVs are facing a major challenge due to the uncertainty in their charging patterns, whereas the distribution grid is mainly designed to serve specific pattern of electric

power demand. The load operation with large current variations contribute to the voltage fluctuations, which adversely lead to light intensity fluctuations. The variations in light (e.g., light flicker) can be characterized by the change in the amplitude and its frequency of occurrence [28]. According to the International Electrotechnical (IEC) vocabulary, the light flicker is defined as "The impression of unsteadiness of visual sensation induced by a light stimulus whose luminance or spectral distribution fluctuated with time" [29]. This may cause irritation to the eye causing what's known as photosensitive epilepsy.

3.2 Definitions and Standards

According to the IEEE std 519-2014 [10], The uses of nonlinear loads connected to the electric power systems include static power converters, arc discharge devices, saturated magnetic devices, and, to a lesser degree, rotating machines. These devices are useful because they can convert ac to dc, dc to dc, dc to ac, and ac to ac. Nonlinear loads change the sinusoidal nature of the ac power current (and consequently the ac voltage drop), thereby resulting in the flow of harmonic currents in the ac power system that can cause interference with communication circuits and other types of equipment. These harmonic currents also lead to increased losses and heating in numerous electromagnetic devices (motors, transformers, etc.). When using the power factor correction capacitors, resonant conditions may occur, which may result in high levels of harmonic voltage and current distortion when the resonant condition occurs at a harmonic associated with harmonic components.

3.2.1 Harmonic (component):

A component of order greater than one of the Fourier series of a periodic quantity. For example, in a 60-Hz system, the harmonic order 3, also known as the "third harmonic," is 180 Hz. The recommended harmonic voltage limits as stated in the standard [10], at the PCC, is 5% at voltage (1 kV < V ≤ 69 kV), while the recommended harmonic current limits at the PCC depends on the ratio (I_{SC}/I_L) short circuit current to the maximum load current. In this thesis, the limit considered when analyzing the harmonic distortion is 5%.

3.2.2 Supraharmonics:

The frequency range above 2 kHz has in the past been considered as "high frequency" for the power quality community and frequencies below 150 kHz have been considered as "low frequency" for those working with EMC issues. But in recent years the frequency range has gained interest from both groups. The term "supraharmonics" has been proposed for any distortion in this frequency range and is getting increasingly used now [17]. The term "Supraharmonics" is often used for components in the frequency range 2 to 150 kHz. The two main sources of supraharmonics, that have been identified, are power-electronic converters with active or passive switching (non-intentional emission) and transmitters of power-line communication (intentional emission). With the introduction of self-commutated valves, emission has shifted from harmonic to supraharmonic frequencies. Products have been designed for satisfying emission limits at harmonic frequencies but instead having increased emission at higher

frequencies. Some examples of devices that have been found to emit supraharmonics are listed below as mentioned in [15]:

• Industrial size converters (9 to 150 kHz).

• Oscillations around commutation notches (up to 10 kHz).

• Streetlamps (up to 20 kHz).

• EV chargers (15 kHz to 100 kHz).

• PV inverters (4 kHz to 20 kHz).

• Household devices (2 to 150 kHz).

• Power line communication, AMR (9 to 95 kHz).

Measurements as well as simulations have shown that the emission from an installation, in the frequency range from a few kHz, is much less than the sum of the emission from the individual devices. Supraharmonic emission tends to flow in between connected devices to a great extent.

3.2.3 Voltage fluctuations:

In electric power systems sometimes give rise to noticeable illumination changes from lighting equipment. The frequency of these voltage fluctuations is much less than the 50-Hz or 60-Hz supply frequency; however, they may occur with enough frequency and magnitude to cause irritation for people observing the illumination changes. This phenomenon is often referred to as flicker, lamp flicker, and sometimes voltage flicker. Often, the terms have been used interchangeably. Some definitions need to be defined in order to measure the level of flickers according to IEEE std 1453-2004 [30].

“ Pst: A measure of short-term perception of flicker obtained for a ten-minute interval. This value is the standard output of the IEC flicker meter.

Plt: A measure of long-term perception of flicker obtained for a two-hour period. This value is made up of 12 consecutive Pst values**.**

The Compatibility level: The specified disturbance level used as a reference level in a specified environment for coordination in the setting of emission and immunity limits. This is normally taken as the level of Pst or Plt above, which customer complaints are likely to occur. These levels are not used for assessing individual load compliance.

Point of Common Coupling (PCC): The point on the MV, HV, or EHV bus on the electric power system electrically closest to a particular fluctuating load, at which point other loads are or could be connected.

Low voltage (LV): Voltage levels that are less than or equal to 1 kV.

Medium voltage (MV): Voltage levels that are greater than 1 kV, but less than or equal to 35 kV. The compatibility level for Pst and Plt for LV and MV power systems”. The flickers levels listed in table 3.1 are recommended and are based on 95%probability levels. These are generally considered to be levels below which there will be no complaints due to voltage fluctuation.

Table 3.1 COMPUTABILITY LEVELS FOR PST AND PLT IN LV AND MV POWER SYSTEMS

Compatibility Levels	
PST	1.0
PLT	0.8

3.3 Low order, high order harmonics calculations.

Harmonic effective root mean square (rms) quantities calculations for low order harmonic (up to 2.4 kHz) and high order harmonics (over 2.4 kHz).

3.3.1 Low and high-order harmonic quantities in three-phase non-sinusoidal situations

In order to assess the harmonic distortion emitted from fast charging stations, the power quantities in three-phase systems at the low-order (ranging from 2^{nd} to 39^{th} harmonic order) and the high-order harmonics (starting from the 40^{th} harmonic order and beyond) are mathematically formulated. Specifically, new three-phase power quantities are defined by separating the low-order harmonics and the high-order harmonics of the non-fundamental effective apparent power (S_{eN}) as shown in figure 3.1.

The effective apparent power (S_e) can be separated to fundamental effective apparent power (S_{e1}) and non-effective apparent power (S_{eN}). The later in turn can be divided into three components, low order harmonic effective non-fundamental apparent power (S_{eNL}) which includes the harmonics from 2^{nd} harmonic order to 39^{th} harmonic order, high order

harmonic effective non-fundamental apparent power (S_{eNH}) that includes harmonics from 40th harmonic order and beyond, and the harmonic interference effective non-fundamental apparent power (S_{eNI}) that result from interaction between the high order and low order harmonic current and voltage distortion components.

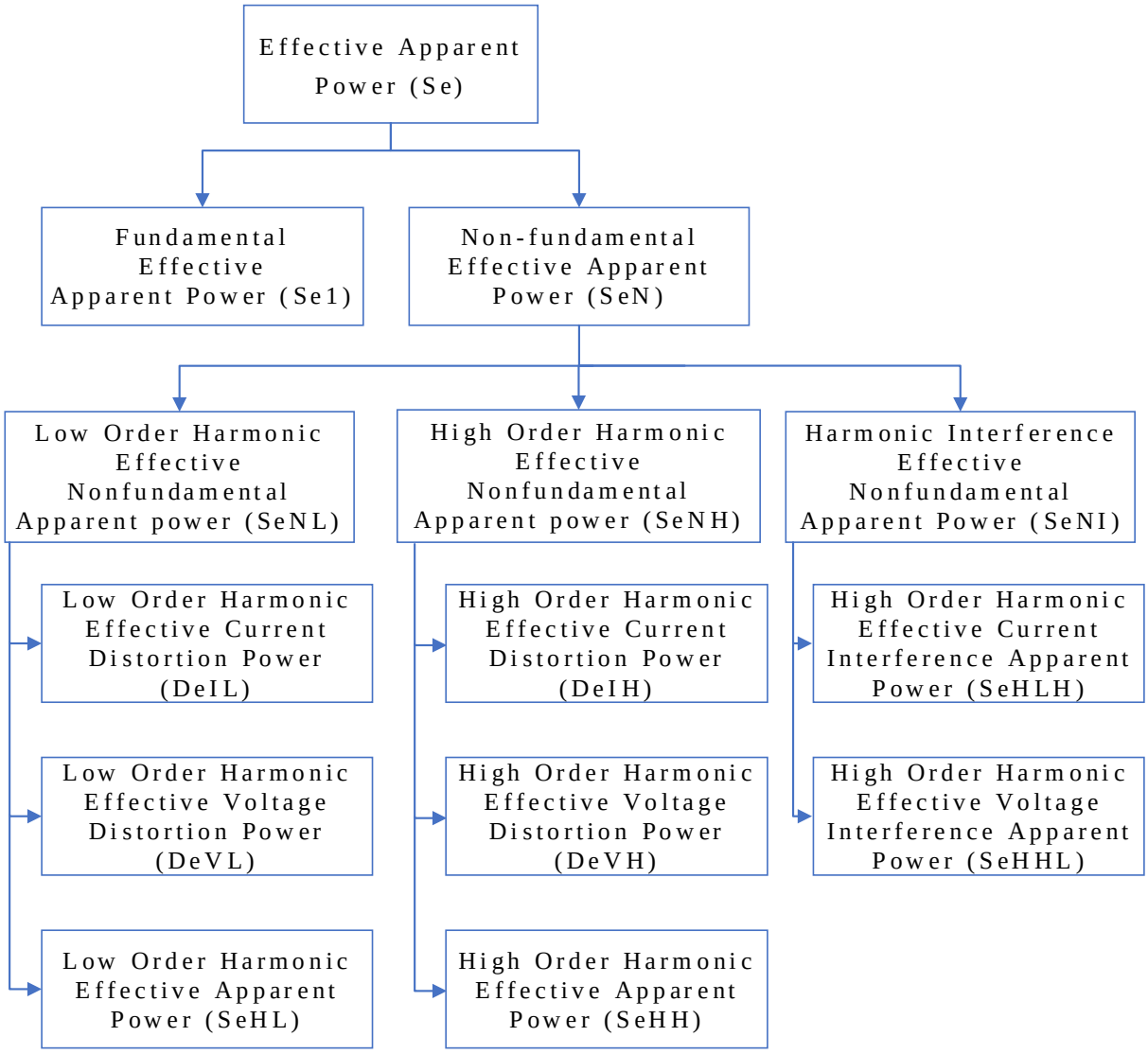

Figure 3.1: Separation of the non-fundamental effective apparent power into low-order and high order harmonic distortion power quantities.

3.3.2 Low and High-order harmonic effective root mean square (rms) quantities

For three-phase systems with phase labels a, b and c, the IEEE Standard 1459-2010 [31] recommends the use of the effective root mean square (rms) voltage (V_e) and current (I_e).

$$V_e = \sqrt{\frac{V_{ab}^2 + V_{bc}^2 + V_{ca}^2}{9}} \tag{3.1}$$

$$I_e = \sqrt{\frac{I_a^2 + I_b^2 + I_c^2}{3}} \tag{3.2}$$

In non-sinusoidal situations, the Standard in [31] recommends the separation of the effective rms voltage and current into two components – the fundamental effective voltage (V_{e1}) and current (I_{e1}) and the nonfundamental effective voltage (V_{eH}) and current (I_{eH}) respectively .

$$V_e = \sqrt{V_{e1}^2 + V_{eH}^2} \tag{3.3}$$

$$I_e = \sqrt{I_{e1}^2 + I_{eH}^2} \tag{3.4}$$

Where

$$V_{e1} = \sqrt{\frac{V_{ab1}^2 + V_{bc1}^2 + V_{ca1}^2}{9}} \qquad V_{eH} = \sqrt{\frac{V_{abH}^2 + V_{bcH}^2 + V_{caH}^2}{9}} \tag{3.5}$$

$$I_{e1} = \sqrt{\frac{I_{a1}^2 + I_{b1}^2 + I_{c1}^2}{3}} \qquad I_{eH} = \sqrt{\frac{I_{aH}^2 + I_{bH}^2 + I_{cH}^2}{3}} \tag{3.6}$$

The non-fundamental in turn can be separated into two components – low-order harmonic (V_{eHL} and I_{eHL}) from 2nd to 39th order and high-order harmonic (V_{eHH} and I_{eHH}), which include all the remaining harmonic order (40th harmonic order and beyond).

$$V_{eH} = \sqrt{V_{eHL}^2 + V_{eHH}^2} \tag{3.7}$$

$$I_{eH} = \sqrt{I_{eHL}^2 + I_{eHH}^2} \tag{3.8}$$

Where, the low and high-order harmonic effective rms voltages are:

$$\mathrm{V}_{eHL} = \sqrt{\frac{V_{abHL}^2 + V_{bcHL}^2 + V_{caHL}^2}{9}} \tag{3.9}$$

$$\mathrm{V}_{eHH} = \sqrt{\frac{V_{abHH}^2 + V_{bcHH}^2 + V_{caHH}^2}{9}} \tag{3.10}$$

and the low and high-order harmonic effective rms currents are:

$$\mathrm{I}_{eHL} = \sqrt{\frac{I_{aHL}^2 + I_{bHL}^2 + I_{cHL}^2}{3}} \tag{3.11}$$

$$\mathrm{I}_{eHH} = \sqrt{\frac{I_{aHH}^2 + I_{bHH}^2 + I_{cHH}^2}{3}} \tag{3.12}$$

With the low and high-order harmonic rms voltage defined as:

$$\mathrm{V}_{abHL} = \sqrt{\sum_{m=2}^{39} V_{abm}^2} \quad , \quad \mathrm{V}_{bcHL} = \sqrt{\sum_{m=2}^{39} V_{bcm}^2} \quad , \quad \mathrm{V}_{caHL} = \sqrt{\sum_{m=2}^{39} V_{cam}^2} \tag{3.13}$$

$$\mathrm{V}_{abHH} = \sqrt{\sum_{m=40}^{\infty} V_{abm}^2} \quad , \quad \mathrm{V}_{bcHH} = \sqrt{\sum_{m=40}^{\infty} V_{bcm}^2} \quad , \quad \mathrm{V}_{caHH} = \sqrt{\sum_{m=40}^{\infty} V_{cam}^2} \tag{3.14}$$

and with the low and high-order harmonic rms current defined as:

$$\mathrm{I}_{aHL} = \sqrt{\sum_{n=2}^{39} I_{an}^2} \quad , \quad \mathrm{I}_{bHL} = \sqrt{\sum_{n=2}^{39} I_{bn}^2} \quad , \quad \mathrm{I}_{cHL} = \sqrt{\sum_{n=2}^{39} I_{cn}^2} \tag{3.15}$$

$$\mathrm{I}_{aHH} = \sqrt{\sum_{n=40}^{\infty} I_{an}^2} \quad , \quad \mathrm{I}_{bHH} = \sqrt{\sum_{n=40}^{\infty} I_{bn}^2}, \quad \mathrm{I}_{cHH} = \sqrt{\sum_{n=40}^{\infty} I_{cn}^2} \tag{3.16}$$

3.3.3 Low and high-order harmonic effective power quantities

In non-sinusoidal situations, the effective apparent power S_e is resolved according to [31] into the fundamental effective apparent power S_{e1} and the nonfundamental effective apparent power S_{eN}.

$$S_e^2 = S_{e1}^2 + S_{eN}^2 \tag{3.17}$$

Where the fundamental effective apparent power

$$S_{e1} = 3V_{e1}I_{e1} \tag{3.18}$$

The non-fundamental effective apparent power is resolved into the effective current distortion power D_{eI}, effective voltage distortion power D_{eV} and effective harmonic apparent power S_{eH}.

$$S_{eN}^2 = D_{eI}^2 + D_{eV}^2 + S_{eH}^2 \tag{3.19}$$

Where, the effective current distortion power D_{eI} and the effective voltage distortion power Dev are defined as:

$$D_{eI} = 3V_{e1}I_{eH} \tag{3.20}$$

$$D_{eV} = 3V_{eH}I_{e1} \tag{3.21}$$

And the effective harmonic apparent power S_{eH}:

$$S_{eH} = 3V_{eH}I_{eH} \tag{3.22}$$

Since the non-fundamental effective voltage and current include the low and high-order harmonics voltages (V_{eHL} and V_{eHH}) and currents (I_{eHL} and I_{eHH}), then using these terms

the power components of the non-fundamental effective apparent power in (3.19) can be resolved into low and high order effective harmonic powers as per [32].

$$S_{eN}^2 = S_{eNL}^2 + S_{eNH}^2 + S_{eNI}^2 \tag{3.23}$$

Where S_{eNL} is the low-order harmonic effective non-fundamental apparent power, S_{eNH} is the high-order harmonic effective non-fundamental apparent power and S_{eNI} is the harmonic interference effective nonfundamental apparent power.

3.3.4 Low and high-order harmonic effective current distortion power

These non-fundamental power components are considered non-active powers and result from the interaction of the fundamental effective voltage with the low-order harmonic effective current (I_{eHL}) and the high-order harmonic effective current (I_{eHH}) respectively.

$$D_{e1}^2 = (3V_{e1}I_{eHL})^2 + (3V_{e1}I_{HH})^2 = D_{eIL}^2 + D_{eIH}^2 \tag{3.24}$$

The low-order harmonic effective current distortion power (D_{eIL}) and the high-order harmonic effective current distortion power (D_{eIH}) identify the segment of the non-fundamental nonactive power due to the low-order and high-order harmonic current distortion respectively.

3.3.5 Low and high-order harmonic effective voltage distortion power

These non-fundamental power components are considered non-active powers and result from the interaction of the fundamental effective current with the low-order harmonic effective voltage (V_{eHL}) and the high-order harmonic effective voltage (V_{eHH}) respectively.

$$D_{eV}^2 = (3V_{eHL}I_{e1})^2 + (3V_{eHH}I_{e1})^2 = D_{eVL}^2 + D_{eVH}^2 \tag{3.25}$$

The low-order harmonic effective voltage distortion power (D_{eVL}) and the high-order harmonic effective voltage distortion power (D_{eVH}) identify the segment of the non-fundamental nonactive power due to the low-order and high-order harmonic voltage distortion respectively.

3.3.6 Low and high-order harmonic effective and interference apparent power

Starting from the effective harmonic apparent power defined in (3.19), the low-order and high-order harmonic effective apparent power can be obtained using the harmonic voltage and currents in (3.7, 3.8).

$$\begin{aligned} S_{eH}^2 &= 3^2 V_{eH}^2 I_{eH}^2 = 3^2 (V_{eHL}^2 + V_{eHH}^2)(I_{eHL}^2 + I_{eHH}^2) \\ &= 3^2 [(V_{eHL}^2 I_{eHL}^2) + (V_{eHL}^2 I_{eHH}^2) + (V_{eHH}^2 I_{eHL}^2) + (V_{eHH}^2 I_{eHH}^2)] \\ &= S_{eHL}^2 + S_{eHLH}^2 + S_{eHHL}^2 + S_{eHH}^2 \end{aligned} \tag{3.26}$$

The first term (S_{eHL}^2) and fourth terms (S_{eHH}^2) in the above equation represent the low and high-order harmonic effective apparent power due to the low-order and high-order

harmonics in the voltage and current alone. On the other hand, the second term (S_{eHLH}^2) represents the high-order harmonic current interference apparent power which is the result of the product of the high-order harmonic effective current and the low-order harmonic effective voltage. The third term (S_{eHHL}^2) represents the high-order harmonic voltage interference apparent power, which is the result of the product of the high-order harmonic effective voltage and the low order harmonic effective current.

3.3.7 Non-fundamental effective apparent power components

The non-fundamental effective apparent power components defined in (3.23), represent the low-order harmonics, high-order harmonics and the harmonic interference effective apparent power. Each effective non-fundamental apparent power component in (3.23) can be used to combine the low-order harmonic effective distortion powers (D_{eIL}, D_{eVL} and S_{eHL}), the high-order harmonic effective distortion powers (D_{eIH}, D_{eVH} and S_{eHH}) and the high-order harmonic effective interference apparent powers (S_{eHLH} and S_{eHHL}).

$$S_{eNL}^2 = D_{eIL}^2 + D_{eVL}^2 + S_{eHL}^2 \tag{3.27}$$

$$S_{eNH}^2 = D_{eIH}^2 + D_{eVH}^2 + S_{eHH}^2 \tag{3.28}$$

$$S_{eNI}^2 = S_{eHLH}^2 + S_{eHHL}^2 \tag{3.29}$$

3.4 Equivalent total harmonic distortion and harmonic pollution factor in three-phase non-sinusoidal situations

In order to assess the harmonic distortion in three-phase non-sinusoidal situations, the equivalent total harmonic distortion (THD_{eI}) is recommended in [10]. The THD_{eI} is the

ratio of the effective rms of the non-fundamental current (I_{eH}) to the effective rms value of the fundamental current (I_{e1}).

$$THD_{eI} = \frac{I_{eH}}{I_{e1}} \tag{3.30}$$

3.5 The harmonic pollution factor (HPF).

Another important factor needs to be defined to quantify the harmonic pollution cause by non-linear load, harmonic pollution factor is defined by the percentage of the non-fundamental (not 60 HZ components) effective apparent power to the fundamental (60 HZ component) effective apparent power

$$HPF = \frac{S_{eN}}{S_{e1}} \tag{3.31}$$

Where S_{eN} is the non-fundamental apparent power, and S_{e1} is the fundamental apparent power

3.6 Supraharmonics distortion

Increasing amount of electronic equipment emit non-eligible levels harmonics frequencies in the kHz range leads to another factor need to be define, supraharmonics. It intensifies the emission of voltage and current harmonics distortion in the frequency range 2-150 kHz as per [15].

The two main sources of supraharmonics, that have been identified, are the power electronic converters with active and passive switching and transmitters of power-line

communication. Products have been designed for satisfying emission limits at harmonic frequencies but instead having increased emission at higher frequencies.

3.7 Voltage Fluctuation and Light Flicker

The load operation with large current variation contribute to the voltage fluctuation and light flicker [11], which can be characterized by the change in the amplitude and its frequency of occurrence. In order to calculate the light flicker, two factors need to be defined and calculated according to IEEE standard 1453-2004 [30]. Firstly, short-term flicker (P_{st}), The measure of severity based on an observation period of ten minutes is derived as follow

$$P_{st} = \sqrt{0.0314P_{0.1} + 0.0525P_1 + 0.0657P_3 + 0.28P_{10} + 0.08P_{50}} \tag{3.32}$$

Where $P_{0.1}$, P_1, P_3, P_{10} and P_{50} are the percentiles of flicker levels exceeded for 0.1%, 1%, 3%, 10% and 50% of the time during the observation period. For smoothing values of the percentiles, the following equations should be used.

$$P_1 = \frac{(P_{0.7} + P_1 + P_{1.5})}{3} \tag{3.33}$$

$$P_3 = \frac{(P_{2.2} + P_3 + P_4)}{3} \tag{3.34}$$

$$P_{10} = \frac{(P_6+P_8+P_{10}+P_{13}+P_{15})}{5} \quad (3.35)$$

$$P_{50} = \frac{(P_{30}+P_{50}+P_{80})}{3} \quad (3.36)$$

Secondly, long-term perception (P_{LT}) is defined as the long-term perception of flicker obtained for a two-hour period. This value is made up of 12 consecutive P_{ST} values per the following formula

$$P_{LT} = \sqrt[3]{\frac{1}{12}\sum_{J=1}^{12} {P_{ST}}_J^3} \quad (3.37)$$

Where *J* is the consecutives number from 1 to 12

3.8 Consequences of harmonics, supraharmonics and voltage fluctuations.

Increasing the harmonics, Supraharmonics and voltage fluctuation in the distribution system has non-neglectable effect on the power quality of the delivered electricity. The overall effect can be described as harmonic distortion. The effects of harmonic distortion may include:

- overheating in plant, equipment and the power cables supplying them, leading to reduced life and sometimes failure. Reduced efficiency in machines and incorrect operation of protective devices is common. The problem can be particularly acute where sensitive medical equipment is being used, harmonics causing errors and possible misdiagnosis [33].

- Non-linear devices exposed to a voltage at a supraharmonics frequency results in currents at other frequencies, typically at integer multiples (i.e. harmonics).
- Distortion of the voltage waveform feeding a device results directly in maloperation of the device.

Several incidents of equipment malfunctioning or behaving in unwanted ways due to the presence of harmonics, supraharmonics and Voltage fluctuations have been reported [34]. Examples include clocks running too fast, hair dryers turning on by them self and flickering lights. In addition, a device subjected to frequencies below 20 kHz (i.e. in the audible range) can produce audible noise due to stimulation of a mechanical resonance. Animals can hear higher frequencies and could therefore be impacted by supraharmonics at even higher frequencies. The main components expected to be damaged by supraharmonics currents, driven by supraharmonics voltages, are the electrolyte capacitors commonly used in EMC filters and as smoothing capacitors connected after a diode rectifier [15]. Currents of any frequency will contribute to the heating of this capacitor.

- Overheating of the distribution transformers, which has effect on the lifetime of the transformers. This could lead to complete failure of the transformers, capacitor and possible damage to other components. The result will simply be that the emission at unwanted frequencies increases.
- Several studies also indicate that high levels of harmonics, supraharmonics voltages at higher voltage levels could result in insulation failures in cables [15].The failures occurred in compact type cable terminations, rated at 24 kV, with resistive/refractive stress grading. The problem was resolved by installing

another type of cable termination, generally called “geometric type”, whose insulation characteristic is expected not to be dependent on frequency. Additionally, various power system components have higher losses (e.g. conduction losses due to the skin effect, eddy current losses in ferrite cores, etc.) for higher frequencies which can cause overheating and accelerated aging.

3.9 Summary:

This Chapter summarizes the aspects of fast charging stations impacts on the distribution system that are relevant to the power quality phenomena. Specifically, harmonics, supra-harmonics and voltage fluctuations and the appropriate mathematical formulations of the power quantities in light of the IEEE standard 1549-2010 are presented. The chapter also sheds light on the relevant power quality standards (ANSI-C84.1-2011 and EN50160) and the recommended limits with respect to these power quality phenomena in the IEEE 519-2014. New power quantities equations have been developed in this chapter to separate low order and high order distortion power and study the interference between them for power and energy. This decomposition will be used in this thesis to quantifying the impact of the large-scale of fast charging stations on the system level.

Chapter 4. Field Measurements

4.1 Introduction

In order to get accurate simulation results in studying the impact of increasing the penetration of the fast charging stations in the distribution system, field measurements are made. The measurements are used to understand the characteristics of the charging profile of the PEV currently existing in the market as well as the high-power fast chargers produced by different manufacturers and which are used in the fast charging stations.

4.2 Electrical Vehicles and the high-power fast chargers

The electric vehicles' profiles used in this study were obtained from real measurement performed at fast charging stations in Ontario, Canada. Three electrical vehicles and two high-power fast chargers from different manufacturers are used in an experimental set-up consisting of battery energy storage system (BESS) and a Drantez Power Quality analyzer [36]. The fast charging stations are supplied from a battery energy storage system (BESS), which includes a 250-kWh battery and an inverter rated 150 kW, 274 V AC, 60 Hz, 3-phase 316 A AC. The high power fast chargers from two different manufacturers, installed in fast charging stations, were used in this work and they are labeled in this study as chargers from manufacturer A and manufacturer B. Both chargers are Level 3, rated at 50 kW with 480 V AC. The PEVs that are used in this study; Chevy Bolt, model 2017 with battery capacity 60 kWh and a driving range 238 miles; Nissan Leaf, model 2012 with battery capacity 24 kWh and a driving range 73 miles and BMW I3, model 2017 with battery capacity 94 kWh and driving range 114 miles as shown in

table 4.1. The measurements were performed using a Dranetz Power Quality analyzer [35] which has 8 channels and is capable of capturing the low-medium-high frequency transients through peak, waveshape, rms duration and adaptive high-speed sampling, as well as power measurements that clearly characterize harmonics, non-sinusoidal, and unbalanced systems. The data were recorded every 30 seconds over a 24 hours period.

Table 4.1 PEV models and battery capacity

EV	Model	Battery Capacity (KWH)	Kilometer driven (KM)
1	Nissan Leaf 2012	24	118
2	Chevy Bolt 2017	60	383
3	BMW I3 2017	33	184

The following procedures are followed during the experimental measurements:

1. Charge Chevy Bolt with charger A and record the charging profile by Dranetz Power Quality analyzer every 30 seconds.
2. Charge Chevy Bolt with charger B and record the charging profile every 30 seconds.
3. Analyze the results obtained in 1 and 2 and identify the charger's manufacturer that inject the highest distortion.
4. Charge Nissan Leaf from the charger identified in step 3, and record the charging profile every 30 seconds
5. Charge BMW i3 the charger identified in step 3, and record the charging profile each 30 seconds.
6. Analyze the results obtained in steps 3 to 5.

The flow charts in figure 4.1 depicts the procedures of the experiment used in obtaining the field measurements

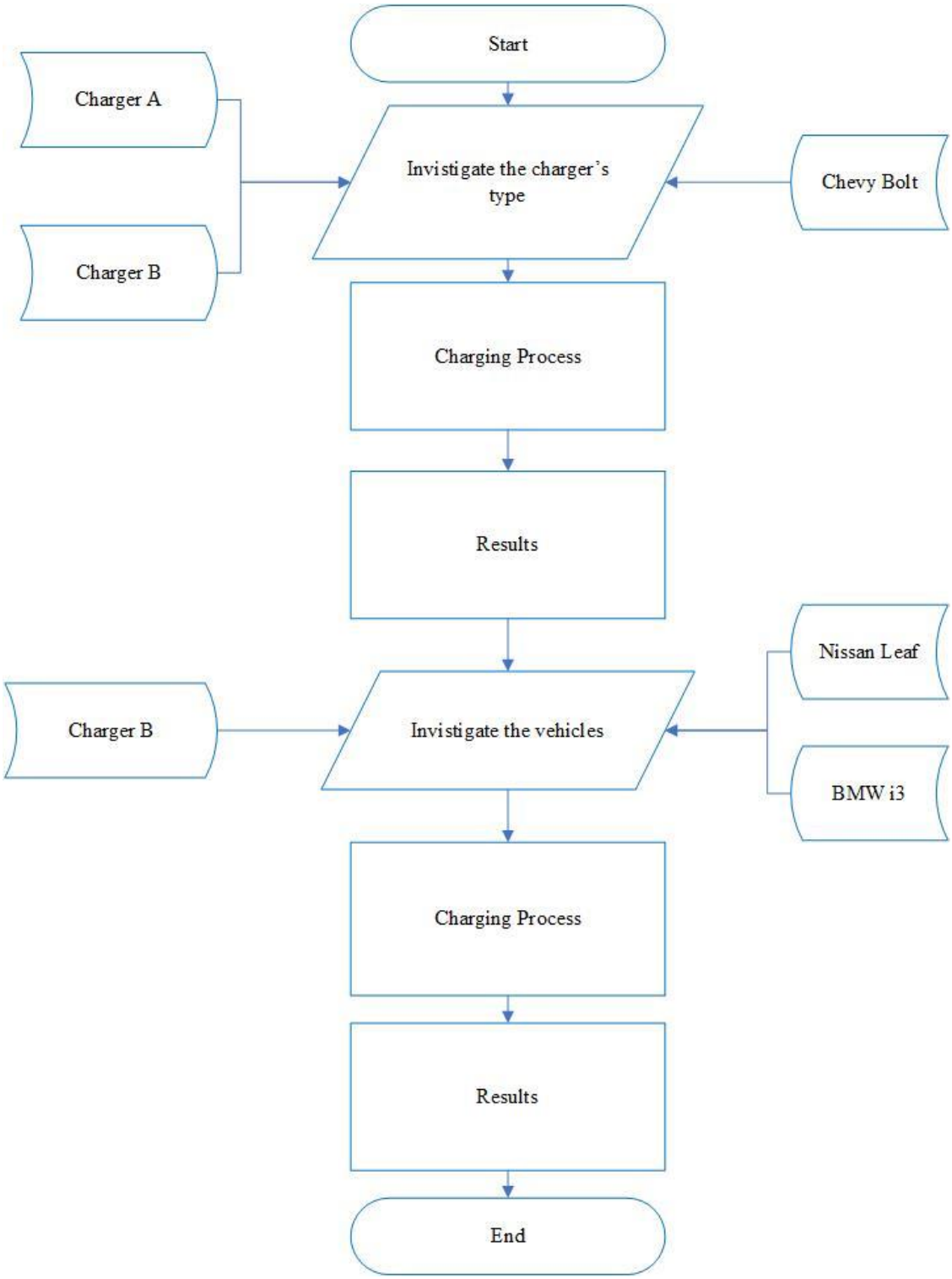

Figure 4.1: Flow chart of the field

The measurement took place every 30 seconds for the charging time of the vehicle in the experiment, as each vehicle has its time of charger depends on the battery capacity of the vehicle. So, it has nearly 120-time step per hour, thus any new change in the profile and harmonics orders can be recorded. The post analysis step is processed after the experiment's measurements have been recorded and it includes the measurements for the total harmonic distortion and the comparison between the charging profiles of the Vehicles with different chargers.

4.3 Results

The results represented in this sections depends on the real measurements which have been measured at the fast charging stations in Canada .

4.3.1 Equivalent total harmonic distortion

In order to examine the impact of increasing the penetration of FCSs on the distribution system in terms of harmonics, the equivalent total harmonics distortion (THD_{eI}) in percent needs to be calculated as described before (3.29). The equivalent total harmonic distortion is calculated each 30 seconds during the charging time of the electrical vehicle in the fast charging station.

4.3.1.1 Equivalent total harmonic distortion (THD_{eI}) at FCS level

The calculations of the THD_{eI} took place at the fast charging station for Charger A and B. The harmonic currents are recorded each 30 seconds for the charging period for each car, and the total harmonic distortion is calculated in each time steps.

Figure 4.2 shows the mean values of the calculated THD_{eI} at the fast charging stations as a comparison between chargers from manufacturer A and B when charging same electrical vehicle Chevy Bolt. It can be noticed that there is a significant difference in the mean value of THD_{eI} measured between charger A and charger B while charging same car Chevy Bolt. The figure reveals that the THD_{eI} for Chevy Bolt charging from charger A is nearly 22 %, while for the same car charging from charger B, the value dropped to around 11%. This result shows that the charger from manufacturer B injects more harmonics compared to the charger from manufacturer A and hence chargers from different manufacturer may have a noticeable effect on the harmonic pollution in the power system.

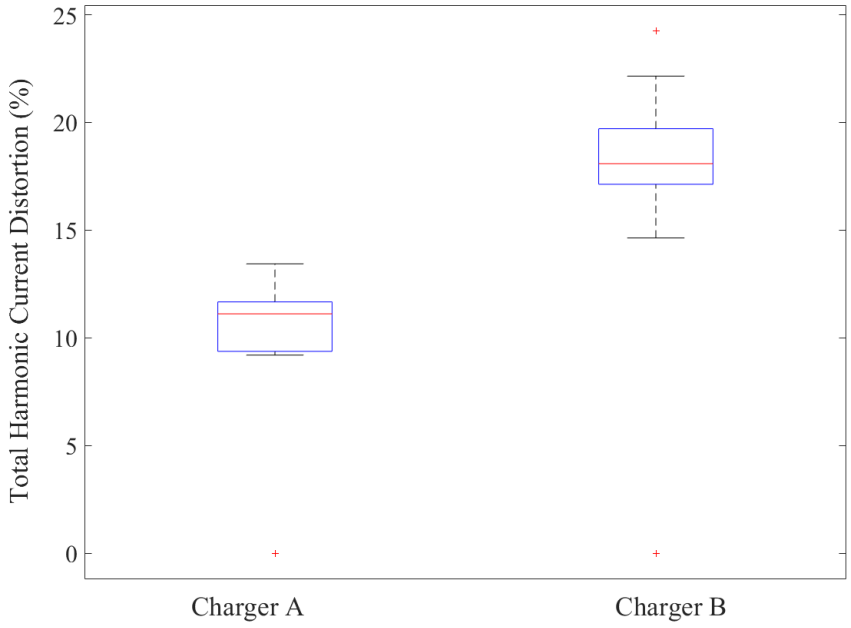

Figure 4.2: Equivalent total harmonics distortion of Chevy Bolt charging from manufacturer A and B

On the other hand, figure 4.3 shows the equivalent total harmonic current distortion (THD_{eI}) calculated in each time step for charging Chevy Bolt, Nissan Leaf and BMW I3 by using charger from manufacturer B.

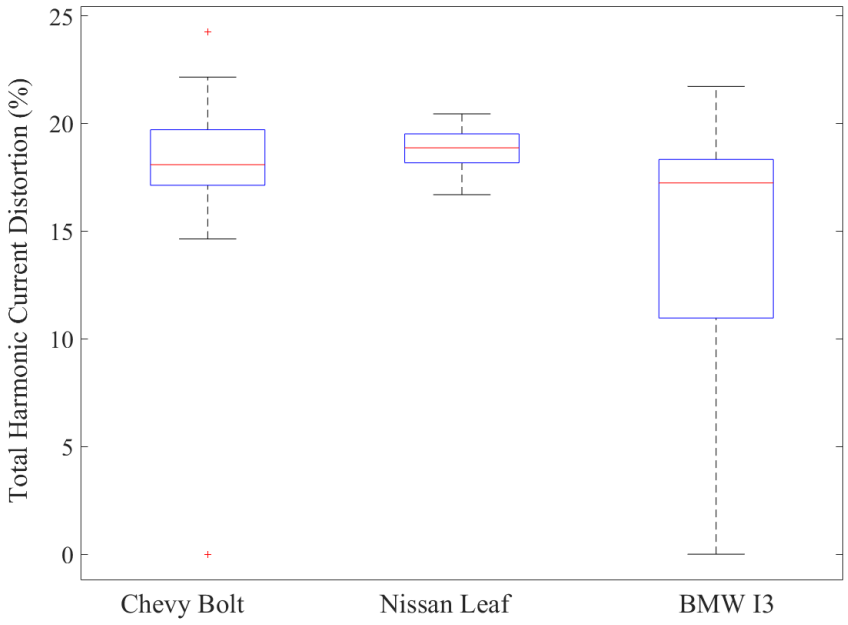

Figure 4.3: Equivalent total harmonics distortion of Chevy Bolt, Nissan LEAF and BMWi3 charging from manufacturer B

It can be seen that the vehicles have slightly difference between each other in the THD_{eI}. The Chevy Bolt has around 18% equivalent total harmonic distortion, while Nissan Leaf contributes around 20%, lastly, BMW i3 has around 16% mean value for the THD_{eI}. Furthermore, for the three types of vehicles charging from different chargers, the calculated THD_{eI} are violating the acceptable level as shown in IEEE-519-2014 [10], which is 5%.

4.3.1.2 Spectrogram of the charging profile

The time-frequency spectrum of the charging current for the two chargers (manufacturers A and B) is shown in figures 4.4 and 4.5 respectively. The horizontal axis labeled time in seconds represents the timed data, which was recorded every 30 seconds, while the vertical axis represents the harmonic order. It can be observed from the figure that the frequency spectra of the two chargers are different. Despite that the chargers from both manufacturers inject more harmonics at the low-order (below 40th harmonic order) than at high-order harmonics (beyond 2.4kHz), the manufacturer B charger injects more harmonics than the manufacturer A charger at the high order while the later inject more harmonics in low order (below 2.4kHz). Specifically, the low-order harmonics are sporadic in case of manufacturer A charger with no significant high-order harmonics while in case of manufacturer B Charger, the high-order harmonics are significant and the low-order are concentrated below the 20^{th} harmonic order (1.2 kHz).

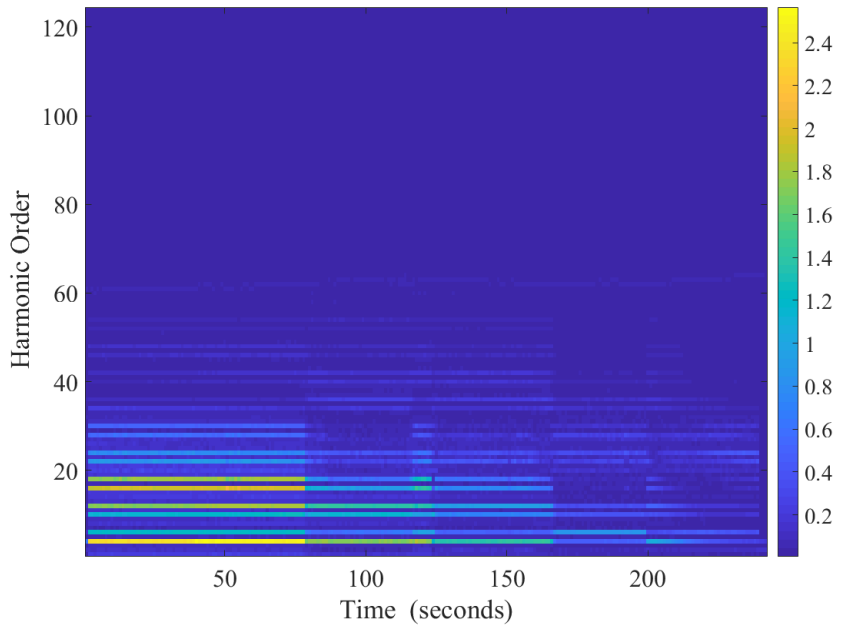

Figure 4.4: Spectrogram of the charging current in case of Chevy Bolt charging from manufacturer A

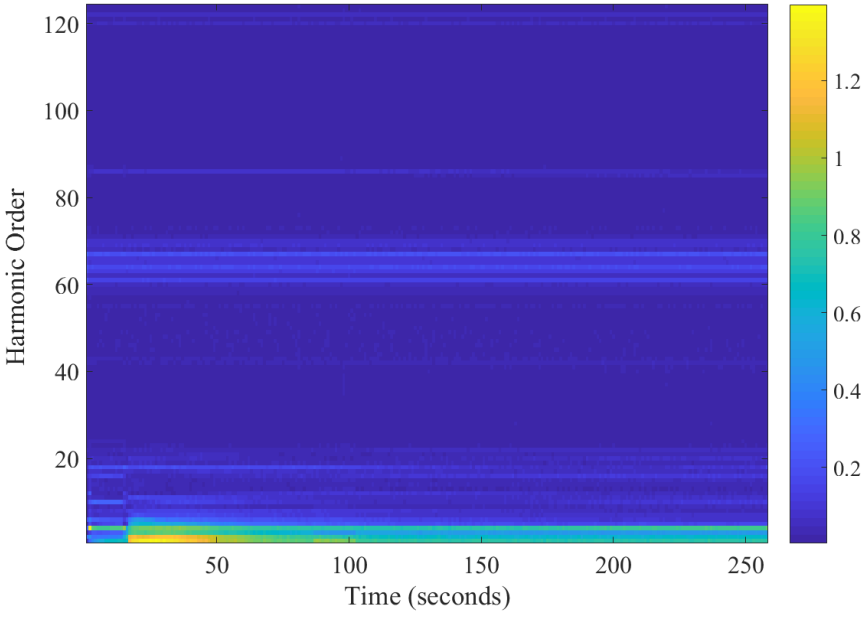

Figure 4.5: Spectrogram of the charging current in case of Chevy Bolt charging from manufacturer B

4.4 Conclusion

The results of the field measurements and the analysis concluded some important points that need more investigation through performing the Monte Carlo simulation. Firstly, Charger B inject total harmonic distortion more than charger A provided charging same car with same conditions as SOC (State of Charge) and same battery capacity. Secondly, although charger B contributes more in the total harmonic distortion, Charger A injects higher magnitude harmonics in the low-order harmonics range compared to that of charger B, while, the later has more harmonic contribution in the high order harmonic range than charger A. Lastly, the harmonic contribution of the PEVs from different manufacturers are different in their harmonic distortion at both the low order and the high order harmonics. Finally, the fast charging stations from both manufacturers are violating the total harmonic distortion acceptable limit from IEEE-519-2014 limits which indicated to be %5.

4.5 Summary

This Chapter describes field measurements that have been performed including three types of electrical vehicles and two different types of fast chargers from different manufacturers. This chapter also shows the impact of PEV charging at the FCS level with different aspects and compare the results with the specified limits in the standards. It shows that chargers from different manufacturers have different harmonic emission in low order and high order harmonics. Besides, the charger's type has more harmonic distortion contribution than electrical vehicle types on the charger's level. The charging

profiles recorded from the real measurements are used in the subsequent chapters to study the impact of the fast charging stations at system level.

Chapter 5. Probabilistic modeling of fast charging stations demand

5.1 Introduction

In evaluating the impact of increasing the penetration of fast charging stations on the distribution systems, an accurate modelling of the electric primary distribution systems should be developed. The power calculations are then used to find the electrical parameters (voltage, current, and power) needed to assess the power quality using the existing indices, which are recommended in power quality standards. This chapter presents an overview of the Monte Carlo simulation used in this work to probabilistically quantifying the impact of integrating high-power fast charging stations in the electric power distribution system.

5.2 Primary Distribution System

The FCSs are typically connected to the primary system of the electric distribution system. The primary distribution system usually starts from the distribution substation and ends at the distribution transformer as seen in figure 5.1. The primary system also includes main and lateral feeders. The main feeder are usually three-phase four wires while the lateral feeder is either single or three phases tapped from the main feeder.

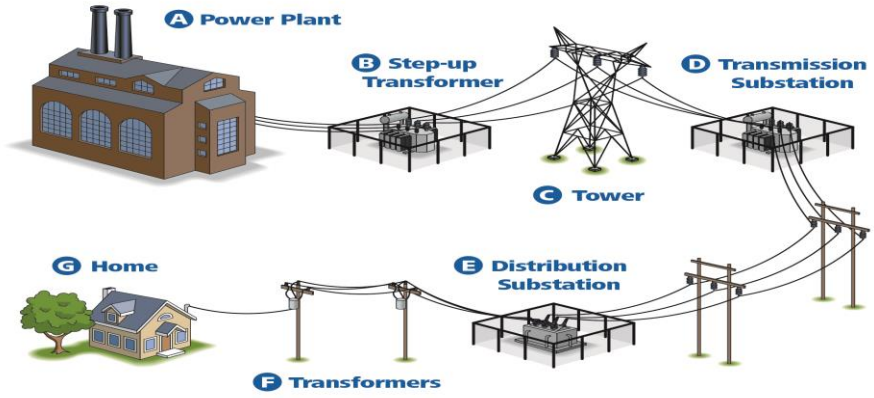

Figure 5.1: Electrical power generation and distribution system

5.2.1 IEEE -34 Node Test Feeder

In 1991 the Test Feeder Working Group (TFWG) released the first set of openly-available distribution test feeder models. This original set of five models was intended to provide researchers with models that included unbalanced loads and non-transposed distribution systems for the purposes of testing new power flow solution methods [36]. The IEEE 34-node test feeder is an actual feeder located in Arizona [37]. The feeder's nominal voltage is 24.9 KV. It is characterized by 1) very long and light loaded, 2) two in-line regulators required to maintain a good voltage profile, 3) an in-line transformer reducing the voltage to 4.16 kV for a short section of the feeder, 4) unbalanced loading with both spot and distributed loads, 5) shunt capacitors. The system has spot loads and distributed loads as listed in Tables 5.1 and 5.2.

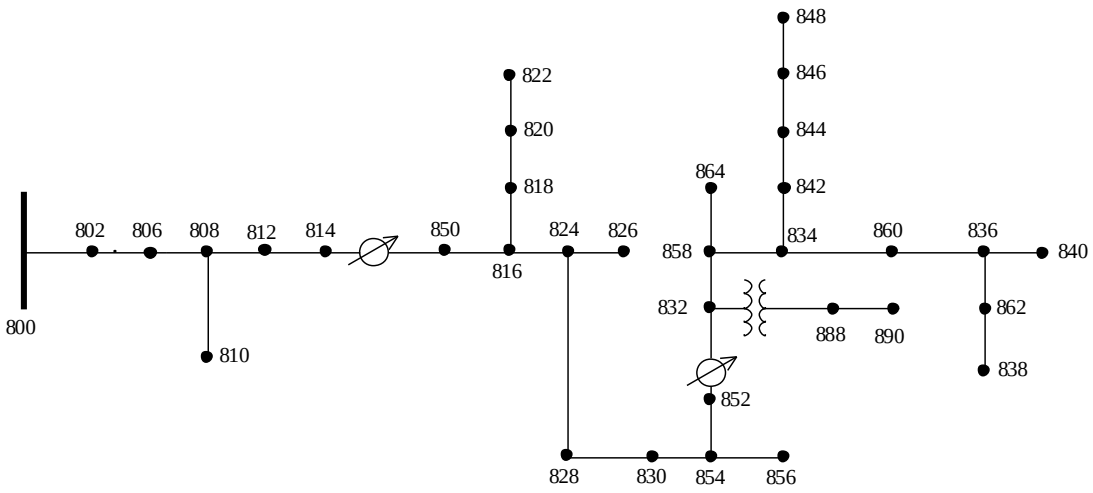

Figure 5.2: IEEE- 34-bus test feeder system

Spot Loads

Node	Load Model	Ph-1 kW	Ph-1 kVAr	Ph-2 kW	Ph-2 kVAr	Ph-3 kW	Ph-4 kVAr
860	Y-PQ	20	16	20	16	20	16
840	Y-I	9	7	9	7	9	7
844	Y-Z	135	105	135	105	135	105
848	D-PQ	20	16	20	16	20	16
890	D-I	150	75	150	75	150	75
830	D-Z	10	5	10	5	25	10
Total		344	224	344	224	359	229

Table 5.1 IEEE- 34-bus test feeder system spot loads details

Distributed Loads

Node A	Node B	Load Model	Ph-1 kW	Ph-1 kVAr	Ph-2 kW	Ph-2 kVAr	Ph-3 kW	Ph-3 kVAr
802	806	Y-PQ	0	0	30	15	25	14
808	810	Y-I	0	0	16	8	0	0
818	820	Y-Z	34	17	0	0	0	0
820	822	Y-PQ	135	70	0	0	0	0
816	824	D-I	0	0	5	2	0	0
824	826	Y-I	0	0	40	20	0	0
824	828	Y-PQ	0	0	0	0	4	2
828	830	Y-PQ	7	3	0	0	0	0
854	856	Y-PQ	0	0	4	2	0	0
832	858	D-Z	7	3	2	1	6	3
858	864	Y-PQ	2	1	0	0	0	0
858	834	D-PQ	4	2	15	8	13	7
834	860	D-Z	16	8	20	10	110	55
860	836	D-PQ	30	15	10	6	42	22
836	840	D-I	18	9	22	11	0	0
862	838	Y-PQ	0	0	28	14	0	0
842	844	Y-PQ	9	5	0	0	0	0
844	846	Y-PQ	0	0	25	12	20	11
846	848	Y-PQ	0	0	23	11	0	0
Total			262	133	240	120	220	114

Table 5.2: IEEE- 34-bus test feeder system distributed loads details

5.2.2 Modeling the distribution system.

In order to assess the impact of EV fast charging stations in term of power quality at the system level, four nodes in the previous system are selected for fast charging stations namely 844, 848, 860 and 890 as shown in figure 5.3. The spot loads at these nodes are replaced by the fast charging stations as listed in table 5.3. Such a choice is made to ensure that the fast charging stations load is equivalent to the original spot load. For example, at node 890, the original spot load is 450 kW, and therefore it is replaced by nine fast charging stations, each rated 50kW (9 x 50 kW = 450 kW).

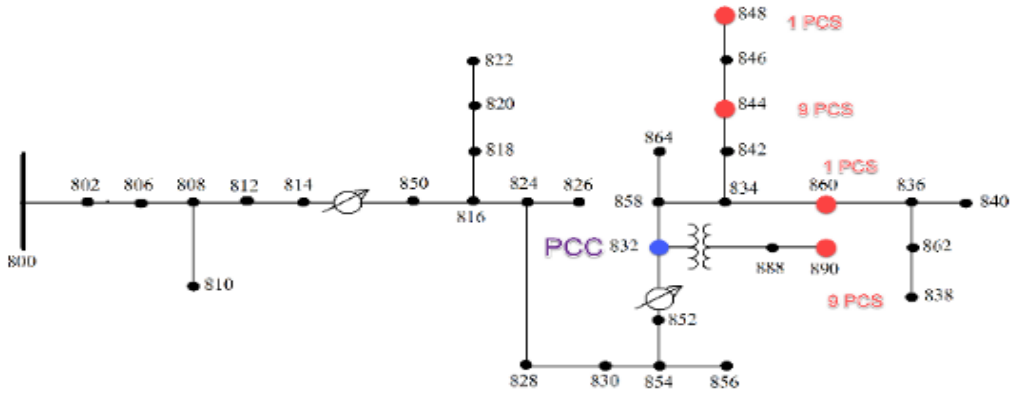

Figure 5.3: IEEE- 34-bus test feeder system with 20 fast charging stations

The total number of fast charging stations in the system is twenty and at each fast charging station the profiles obtained from the real measurements were used following Monte Carlo method to probabilistically estimate the impact of harmonic distortion at the system level.

Table 5.3 IEEE 34 bus test feeder spot loads with FCS replacements

Node number	Spot load (KW)	Voltage (Kv)	No. of FCS	Replacement Load (KW)
860	60	24.9	1	50
844	450	24.9	9	450
848	60	24.9	1	50
890	450	4.16	9	450

5.3 Arrival Time Distribution

In order to simulate the impact of increasing the penetration of the fast charging station on the primary distribution test system, the arrival time of the EVs to the FCSs need to be define for one day (24 hours). The arrival time distribution is adapted from [38] and shown in figure 5.4.

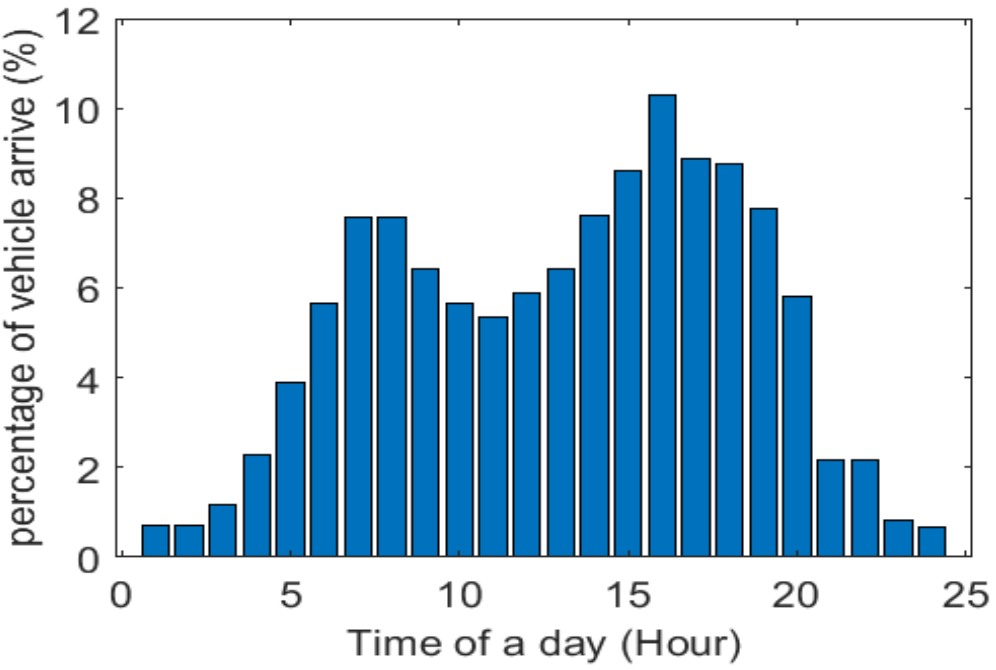

Figure 5.4: The expected arrival time distribution

The distribution depends on the arrival time of the vehicles in the traditional fueling stations. From the figure, it can be noticed that the number of vehicles arrive to the charging station are different during the day, it increased at the rush hours from 6am to 8am at the morning and increase again from around 3pm to 6 pm afternoon. In this study, the arrival time graph is used to estimate the number of EV arrive at the FCS hourly.

Since, only twenty fast charging station in the system exists and the maximum percentage in the arrival time distribution is ten percent, thus the maximum number of PEV can be adapted in this study are two hundred vehicles. Therefore, the number of PEV that may arrive to the FCS hourly can be calculated. For example, there will be around twenty EV may arrive at 4 pm, similarly, at 10 am, there may be around 12 PEVs in the charging stations.

As this work depends on the arrival time distribution, which represents the number of vehicles arriving at the FCS per hour, thus the simulation will change the number of vehicles hourly as well. That means, if the vehicle reaches at 10:30 am, it must wait half an hour so it can be charged at the station. Despite that, the calculation is taking place every 30 seconds of the simulation. Therefore, 60 records in total per hours (2,880 value per day), so it can record any event while charging of the electrical vehicle.

5.4 Monte Carlo Simulation to estimate the FCSs' profiles

After having modeled the distribution system with the fast charging stations inserted in the system, the fast charging stations profile is superimposed on the existing loads demand and need to be simulated at the system level. Monte Carlo Simulation (MCS) is used to probabilistically quantify the impact of large-scale of fast charging stations on the power quality of the power distribution system. In term of low-order harmonics, high-order harmonic namely Supraharmonics and voltage fluctuations by probabilistically estimate the random variables of the charging profile of the electrical vehicles in the fast charging stations .

5.4.1 Introduction

Monte Carlo simulation are a subset of computational algorithms that use the process of repeated random sampling to make numerical estimations of unknown parameters. They allow for the modeling of complex situations where many random variables are involved and assessing the impact of risk. The uses of MC are incredibly wide-ranging and have led to several ground-breaking discoveries in the fields of physics, game theory, and finance. There is a broad spectrum of Monte Carlo methods, but they all share the same principle that consist of performing many simulations for probabilistic analysis. Through repeating an experiment with randomness, the effects of randomness are lessened to an extent where analysis can be drawn to the probabilities of event occurring; such is the basis of Monte Carlo analysis. Through performing multiple trials, Monte Carlo generates the sizable amounts of data with which to analyze accordingly. Given the variety of random number generation schemes used in Monte Carlo simulations, this work utilizes the inversion method. Inversion random number generation involves the sampling of a uniform random number U in the range (0,1) with one-to-one correlation into cumulative distribution function F such that sample X=F-1(U).

One of the most important factors in MCS is the termination criteria at which the MC algorithm stops. The number of MC trials usually affects the quality of the solution. For example, a very low number of trials may lead to large variance in the results and hence poor-quality solution. On the other hand, a very large number of trials more than necessary may not add much value to the analysis, and results in longer computational time and massive data size. In this work, the standard deviation of the point of common coupling effective current is recorded while changing the number of Monte Carlo trials

up to 250 trials. The results reveal that as the number of iterations increases, the change in standard deviation and hence the bus current start to smooth, which indicates the Monte Carlo solution has reached convergence. After 200 trials no significant change in the standard deviation was observed.

5.4.2 Probabilistic estimation of the FCS charging demand.

To examine the impacts of the charging profile of the EVs in the FCSs, the state of charge of the electrical vehicle upon arrival need to be predefined upon arrival of the vehicle to the charging station. Since the vehicles arriving to the charging station have different state of charge (SOC), the time to charge needed for each car is different for the vehicles even if they are of the same type. For example, if the vehicle arrives at the charging station with five percent of SOC, it will need more time to charge than if it arrives at the charging station with 65% SOC. Some vehicles will need less than one hour to charge the battery to 95% while, other will need more than one hour to fully charge the battery. The time to charge each vehicle is estimated based on the remaining state of charge (SOC) of each vehicle when arriving at the FCS using Monte Carlo (MC) method.

The MC method is used to randomly assign SOC for each vehicle arrived at the FCS every hour. Hence upon the arrival of each EV, the portion of the charging profile obtained from the real measurement and which corresponds to the estimated SOC is then loaded at the FCS of the test system.

In each Monte Carlo trial, the EV profiles are used to calculate the currents in the test system feeders and the power quantities at the low-order and high-order harmonics are evaluated as explained in Ch 3 Section 3.3. This process is repeated, until the

convergence occurs. To test the Monte Carlo convergence, the average value of the effective current is calculated at the point of common coupling (PCC, node 832 in figure 5.4), and is compared to the value of the previous trial. This process sis repeated until no further change in the value is noticed with any further increase in the number of iterations, which signifies the convergence is achieved. The convergence test is checked for all scenarios of the simulation system. Firstly, charging Chevy Bolt with charger from manufacturer A, secondly, charging Chevy Bolt from charger from manufacturer B, thirdly, charge Nissan Leaf from charger from manufacturer B, lastly, charge BMW i3 from charger B. The following figures shows the value of the average current measured at the point of common coupling after each iteration. One iteration runs the simulation for 24 hours simulation using the arrival time distribution in figure 5.4, and the calculation took place every 30 seconds and record the average current for the PCC at the end of each iteration. All the simulations run for 300 iterations.

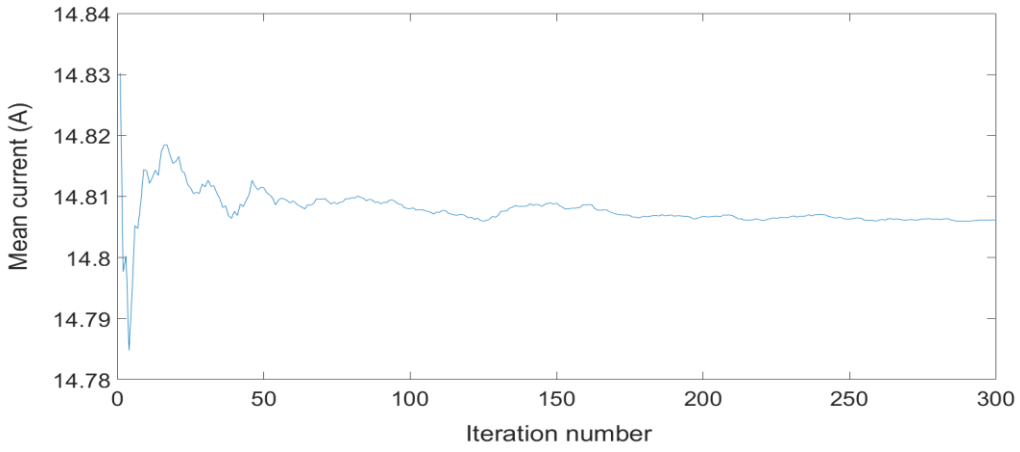

Figure 5.5: Monte Carlo convergence of the mean current at the PCC (node 832) for Chevy Bolt in charger A

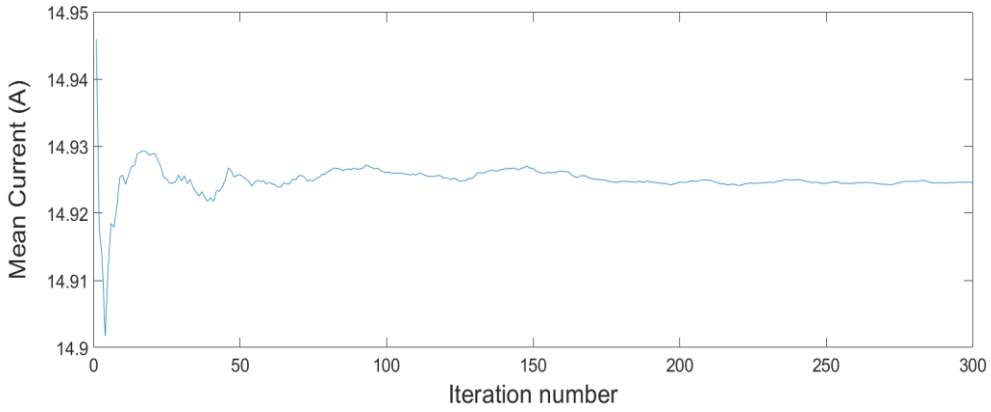

Figure 5.6: Monte Carlo convergence of the mean current at the PCC (node 832) for Chevy Bolt in charger B

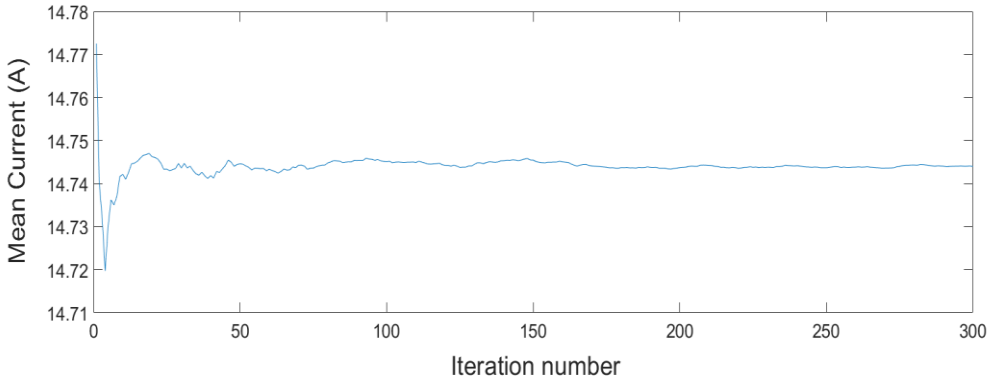

Figure 5.7: Monte Carlo convergence of the mean current at the PCC (node 832) for Nissan Leaf in charger B

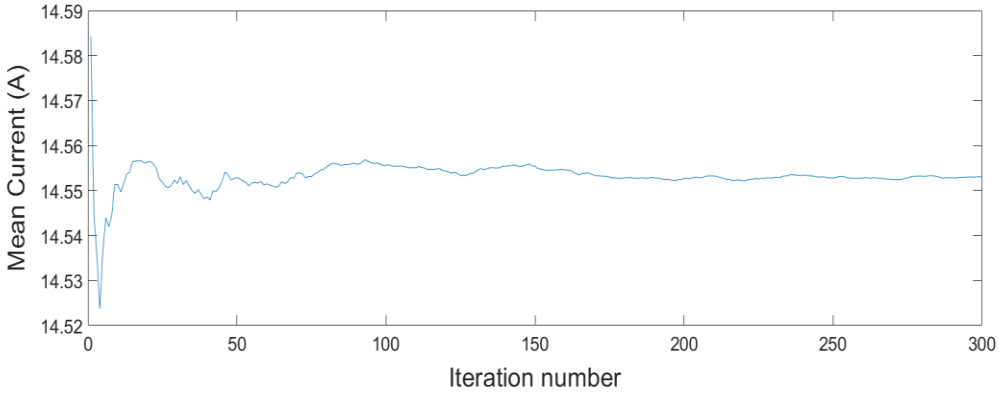

Figure 5.8: Monte Carlo convergence of the mean current at the PCC (node 832) for BMW I3 in charger B

Figures 5.5 -5.8 show the change in the mean value of the current at PCC (point of common coupling), and the figures show that increasing the number of trials beyond a certain value in each simulation does not lead to any significant change in the current value. For example, in figure 5.5, when charging Chevy Bolt in charger A, it can be noticed that after 180 iterations, the value of the current does not change significantly with increasing the number of iterations over 180. Similarly, the convergence was achieved after 200 iterations for test 2, Chevy Bolt in charger B. For test 3, Nissan Leaf in charger B, nearly 100 trials are enough to reach the convergence for MC simulation. Lastly, BMWi3 in charger B as in figure 5.8, the MC simulation will reach the convergency after 160 trials. In this study, 250 iterations were considered in order to ensure that the convergency condition will be achieved and the calculations that depend on the MC simulation results are accurate.

The error of MC simulation is calculated after the termination condition is achieved by the difference between the calculated mean effective current (I_{ec}) value at the PCC node when the convergence occur and the real value of the mean current value (I_e)

$$E_{MC} = \% \left| \frac{I_{ec} - I_e}{I_e} \right| = \frac{\sigma I_e}{\sqrt{N}} \qquad (5.1)$$

Where σ is the standard deviation of the result and N is numbers of trials.

The error is calculated with the above equation after 250 iteration is 0.00175 %.

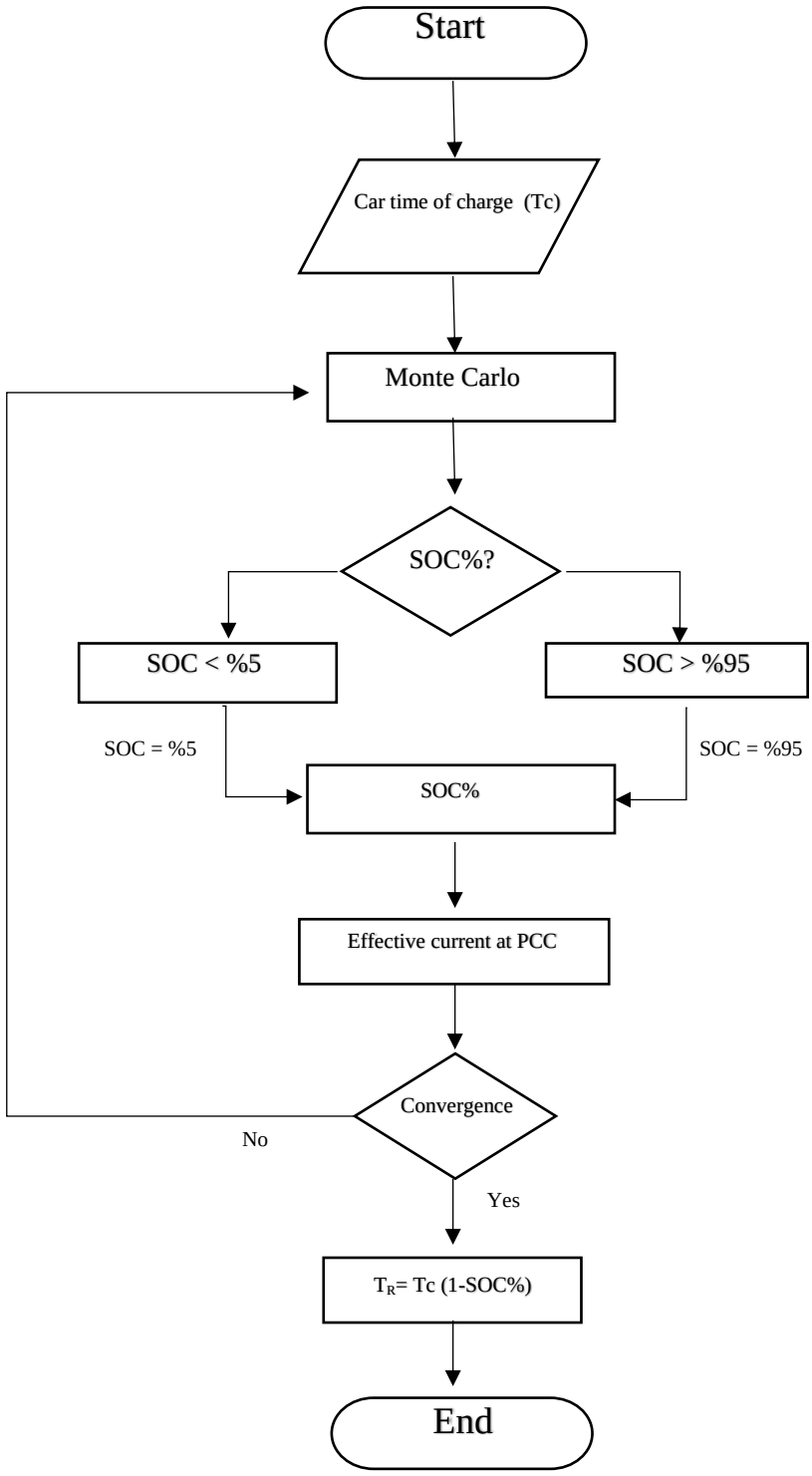

Figure 5.9 : flow chart of using MC to probabilistically estimate the SOC of the arriving vehicles to the FCSs

The flow chart in figure 5.9 represented the procedures of using Monte Carlo technique to probabilistically estimate the random variables needed for estimate the charging profile of the electrical vehicles form the fast charging stations, hence, the power required by each vehicle and the time required (T_R) by each car to charge the battery from the current state of charge to full. And it's calculated from the known charging time of the vehicle (T_C) upon arrival and the estimated state of charge after convergency.

5.5 Summary

This Chapter describes the modeling of the electric primary distribution system components, including the primary system circuits and the spot loads. Modeling of the fast charging stations is presented by replacement of the current spot loads with the equivalent power FCSs, which consists of twenty fast charging stations. This chapter also presents the use of the Monte Carlo method to probabilistically estimate the random variables needed in order to estimate the charging profile of the electrical vehicles arriving to the fast charging stations. This chapter also explained the Monte Carlo convergence algorithm as well as the error measurements. After establishing the simulation system with all measurements aspects, the simulation will be run until convergency is satisfied, then results will be presented in the subsequent chapter.

Chapter 6. Simulation Result and analysis

6.1 Introduction

The purpose of this chapter is to present and analyze the results from applying Monte Carlo Simulation to assess the impact of increasing the penetration of fast charging stations on the power quality in electric distribution system. Specifically, the presented analysis focuses on evaluating the power quality at different penetrations of different types of electrical vehicle charging from different manufacturers' chargers. The chapter starts by describing the simulation system, followed by the modelling of the fast charging stations in the test system. Different combination of electrical vehicle types and charger type, reaching to the result and finally the conclusion of the work.

6.2 Equivalent total harmonic distortion (THD_{eI}) at simulation level.

To study the effect of the real measurements in this study on the system level, the simulation system of IEEE 34 bus test feeder is used with the FCSs as explained in chapter 3. The simulation took place for 24 hours, one day, using the expected arrival time of the car in figure 6.1. The measurements are executed every 30 seconds to reflect the measured profile of the charging vehicles at the FCSs. The total number of vehicles simultaneously charging in the system is 20 vehicles. Upon arrival, the expected SOC for each car is calculated using MC simulation and the time required for charging the vehicle is estimated. This process is repeated, and the mean value of the calculated current at the PCC is recorder and compared with the previous value until the convergence occurs and the termination condition of MC simulation is achieved. Thus, the measurement took place with the expected SOC for each car every 30 second for one

day. Thus, number of EVs reach the charging stations is obtained from the distribution each hour, and vehicles are distributed on the FCSs in order from FCS number 1 to 20. The charging profile for each car corresponds to the SOC of the car is loaded to the FCSs using MATLAB, which is connected to OpenDSS to perform the calculations. The time of charging each vehicle is calculated and at each hour the charging status of the vehicles are examined. In each simulation, all the chargers are assumed to be from one manufacturer and all vehicles are of the same type. This will ensure that the effect of each charger will be studied separately. For example, simulation 1 includes Chevy Bolt charging from Manufacturer A chargers while in simulation 2, Chevy Bolt charging from manufacturer B chargers are used. In simulation 3, Nissan Leaf charging from manufacturer B charger are used while in simulation 4, BMW I3 charging from manufacturer B chargers are used. The reason for these choices is provide a comparison between chargers from manufacturer A and B in charging same PEV which Chevy Bolt, and later, more investigation is needed for charger B, three types of vehicles are charging from charger B to investigate the difference between vehicle's types.

Figures 6.1 and 6.2 show a box plot of the equivalent total harmonic voltage and current distortion respectively, calculated at the PCC point each 30 seconds for 24 hours, in case of charging Chevy Bolt from charger from manufacturer A.

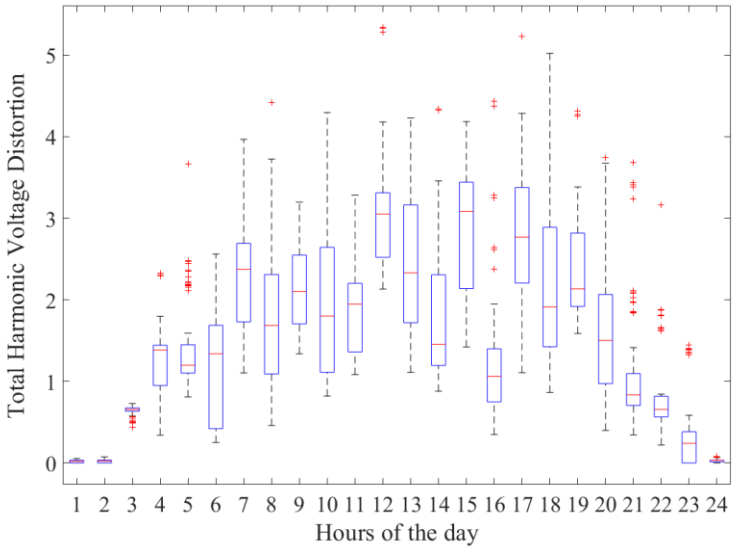

Figure 6.1: Equivalent total harmonic voltage distortion for Chevy Bolt in charger A

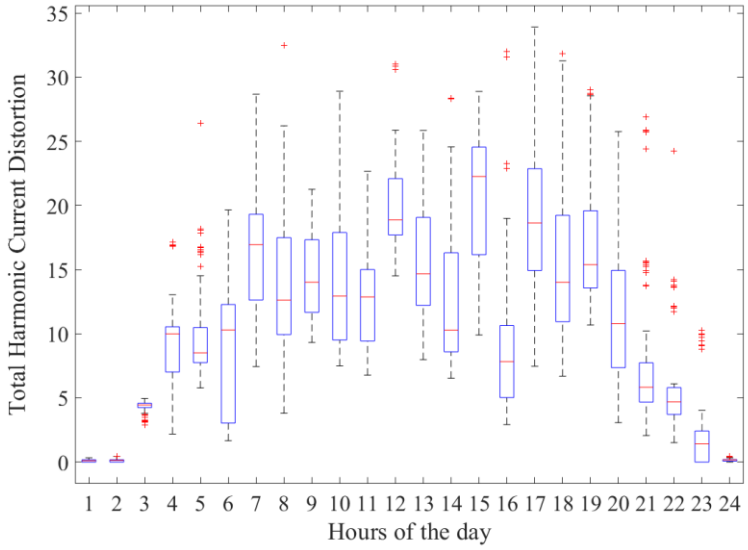

Figure 6.2: Equivalent total harmonic current distortion for Chevy Bolt in charger A

It can be noticed that the current distortion violates the limits of IEEE standards [10], which is 5%. The mean value was around 11 % while the maximum value was around 23% which are higher than the limit which is 5% for this distribution system. On the

other hand, the harmonic voltage distortion is not recording any violation above the limits.

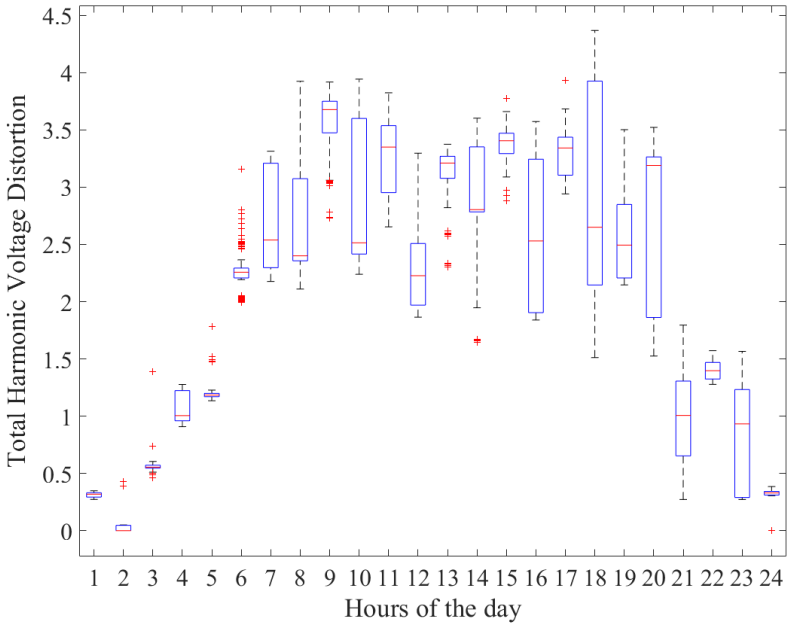

Figure 6.3: Equivalent total harmonic voltage distortion for Chevy Bolt in charger B

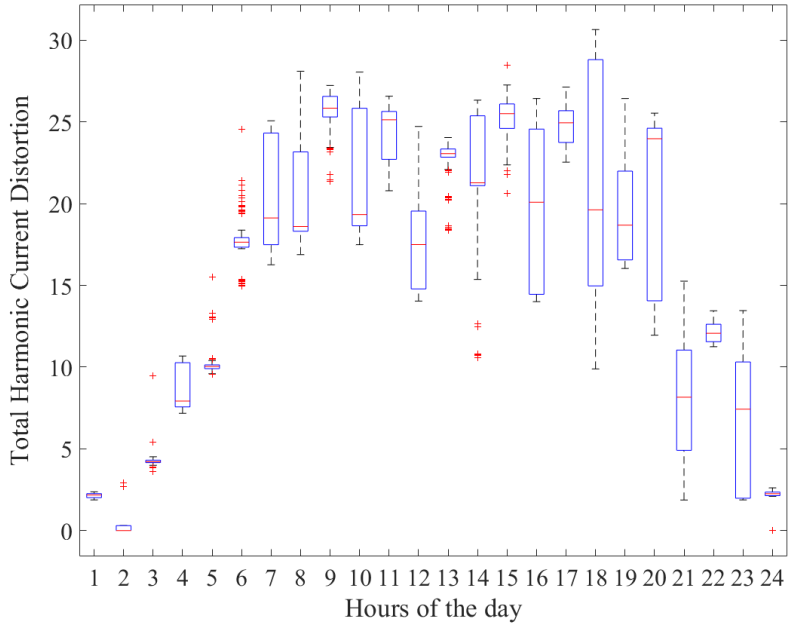

Figure 6.4: Equivalent total harmonic current distortion for Chevy Bolt in charger B

Figures 6.3 and 6.4, show the equivalent total harmonic distortion in the voltage and current when charging Chevy Bolt from manufacturer B charger. The figures reveal that there is a clear violation in the equivalent total harmonic current distortion during the day as it reaches around 26% with the 50^{th} percentile around 23%, while the total harmonic voltage distortion was within the limit.

On the other hand, comparing figure 6.3 and figure 6.5, it can be noticed that although charging same kind of vehicle Chevy Bolt in both cases, the equivalent total harmonic distortions are different in both cases depending on the chargers' types. Charger B contributes more harmonic distortion in the distribution system compared to that of charger A.

Table 6.1 Total equivalent harmonic current distortion (%)

Scenario	THDI (%)
1	11
2	23

This result reveals that charger from manufacturer B injects more harmonics compared to the charger from manufacturer A and hence chargers from different manufacturers may have a noticeable effect on the harmonic emission. For more investigating for harmonic distortion emitted from charger B, two more types of vehicles have been placed to be charging from charger from manufacturer B, Nissan Leaf and BMW i3.

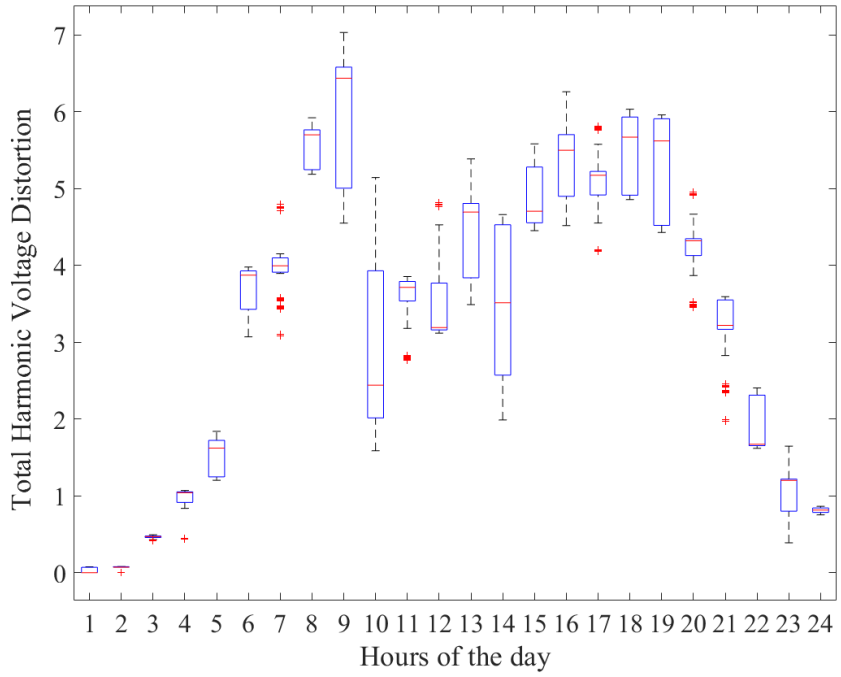

Figure 6.5: Equivalent total harmonic voltage distortion for Nissan Leaf in charger B

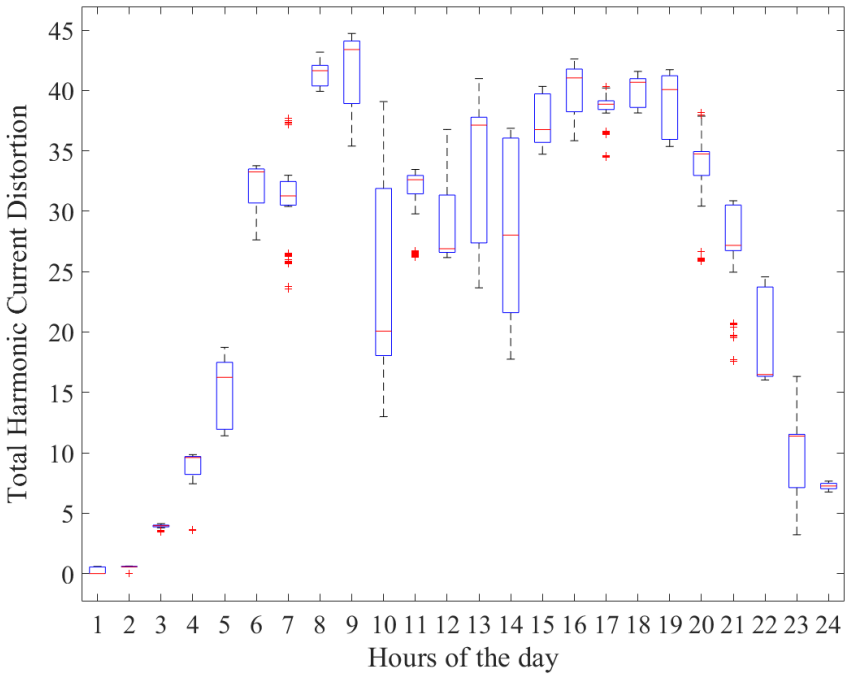

Figure 6.6: Equivalent total harmonic current distortion for Nissan Leaf in charger B

The box plot shown in figures 6.5, 6.6 show the equivalent total harmonic voltage distortion (THD_{eV}) and the equivalent total harmonic current distortion (THD_{eI}) of using electrical vehicle, Nissan Leaf, and use charger from manufacturer B as FCS in the simulation. The figure reveals that the voltage and current distortion in this case are higher than the case of using Chevy Bolt with same kind of charger B in figures 6.3, 6.4. The equivalents total current distortion reaches the maximum of 41% during one day with 50^{th} percentile of 27 %, while the equivalent total harmonic voltage distortion violate in same times during the day the limit of the voltage distortion as per IEEE standards 5% [10].

Similarly, using BMW i3 electrical vehicle with same charger B, for 24 hours with calculation performed each 30 seconds, the results can be seen in figures 6.8, 6.9.

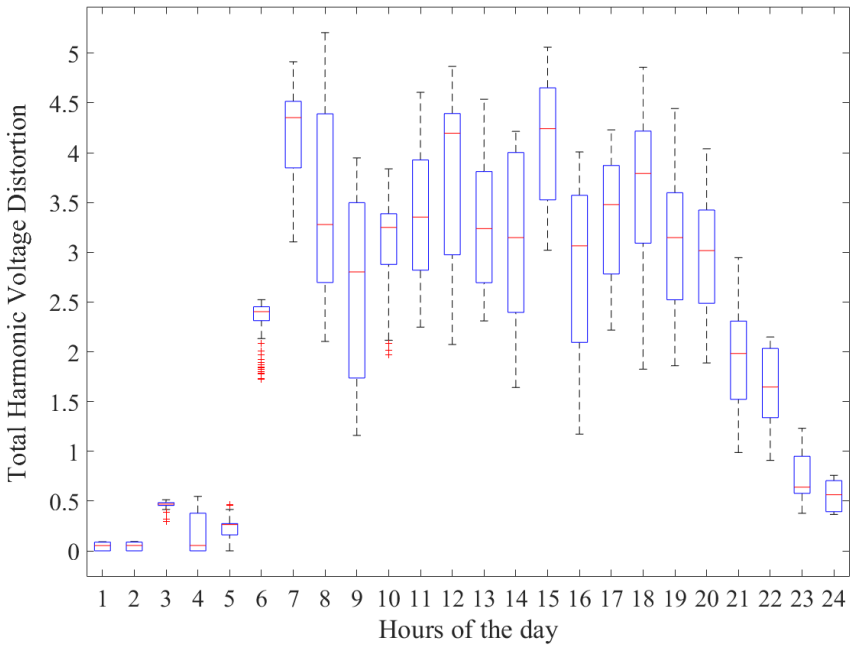

Figure 6.7: Equivalent total harmonic voltage distortion for BMWi3 in charger B

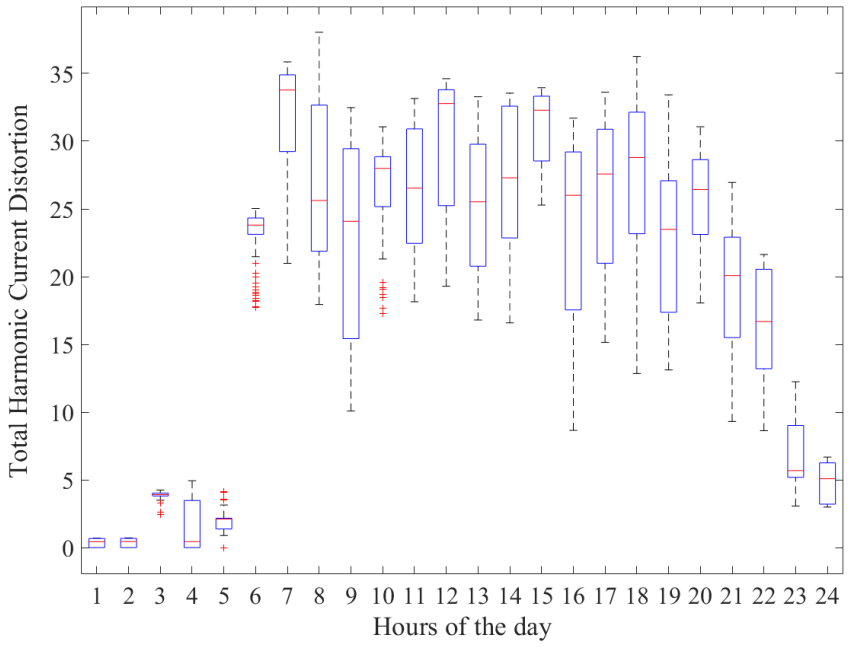

Figure 6.8: Equivalent total harmonic current distortion for BMWi3 in charger B

From the figures, it can be observed that the equivalent total harmonic current distortion is violating the limit in case of charging BMW i3 electrical vehicle in Charger B. It reaches maximum value of 35% with the 50^{th} percentile of 24%, while the equivalent total harmonic voltage distortion is within the limit during the full simulation for one day.

To sum up the results of the total harmonic distortion, table 6.2 indicates the equivalent total harmonic distortion for the voltage and current for Chevy Bolt in Charger A and B, Nissan leaf and BMW i3 in charger B.

Table 6.2 Total equivalent harmonic distortion (%)

Test Description	THD_{eV}(%)	THD_{eI} (%)
Chevy/Charger A	2	11
Chevy/Charger B	2.5	23
Nissan/ Charger B	4.5	27
BMW/ Charger B	3	24

From the table, it can be noticed that charger B inject more current harmonics in the power system than charger A. Besides, the electrical vehicles are different in harmonic emission depends on the type of the vehicle although using same charger.

On the other hands, the recorded equivalent total harmonic current distortion for the four simulation tests are violating the upper limit of IEEE standard for the approved limits of total harmonic current distortion, which is 5% [10]. Besides, some violations recorded for the equivalent total harmonic voltage distortion in case of using Nissan Leaf with charger from charger B.

6.3 Three-phase power quantities in case of PEV fast chargers

The three-phase power quantities explained in Chapter 3 Section 3.3, are computed and compared for the chargers from the two different manufacturers. In order to see the effect at the system level, the results obtained at the point of common coupling (node 832) are presented at a 30 second resolution for a 24 hours period.

6.3.1 Low-order harmonic effective current distortion power

The Box plot in figure 6.9 and 6.10 represent the low-order harmonic effective current distortion power (D_{eIL}) and energy in var.sec respectively, at the PCC (point of common coupling) (node 832) in case of chargers from manufacturer A and manufacturer B.

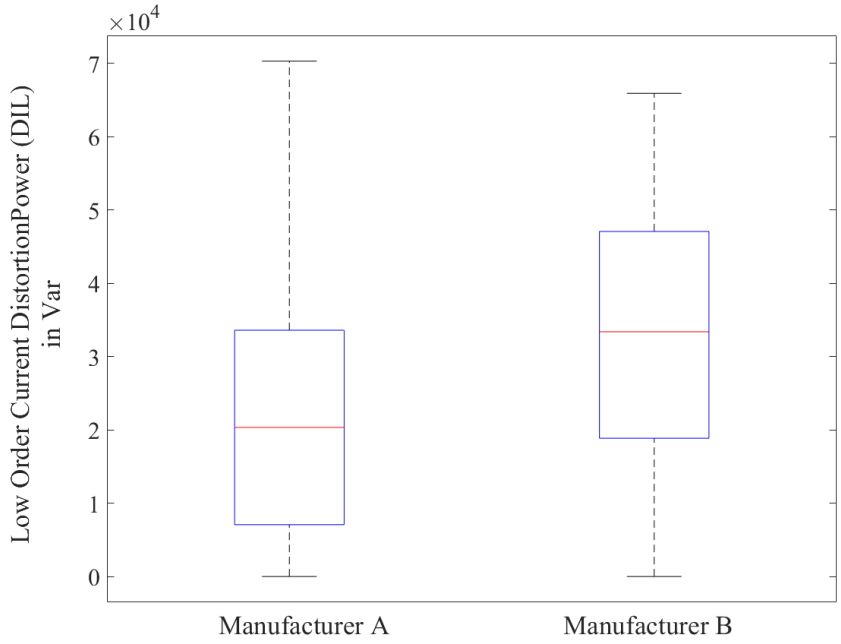

Figure 6.9: Low order Harmonic current distortion power

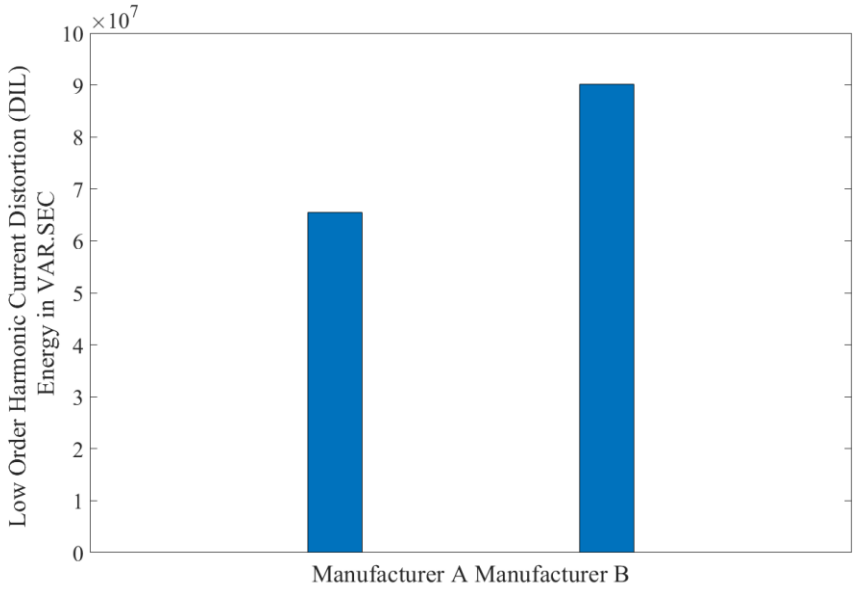

Figure 6.10: Low order Harmonic current distortion energy

The figures reveal that the current distortion power at the low-order harmonic is greater in case of manufacturer B charger compared to manufacturer A charger and hence the amount of current distortion energy at the low-order harmonics in case of manufacturer B charger is higher compared to manufacturer A charger. Thus, it can be inferred that manufacturer B charger contributes larger amount of nonfundamental non-active distortion at low-order harmonic current than manufacturer charger A charger, which in terms of the current distortion energy, manufacturer B charger measures 97 Mvar.sec while manufacturer A charger measures 62 Mvar.sec.

6.3.2 High-order harmonic effective current distortion power

The plots of the harmonic effective current distortion power (D_{eIH}) and energy for high-order harmonic (above 40th order) are shown in figure 6.11 and 6.12 respectively. It can be observed that manufacturer B charger contributes more in terms of the high-order effective current distortion power and energy compared to manufacturer A charger. The 50th percentile of the high-order harmonic effective current distortion power of manufacturer B charger measures 2 kvar while in case of manufacturer A charger, it measures 0.8 kvar. Consequently, the high-order harmonic effective current distortion energy measures 5 Mvar.sec and 3 Mvar.sec for chargers from B and A respectively.

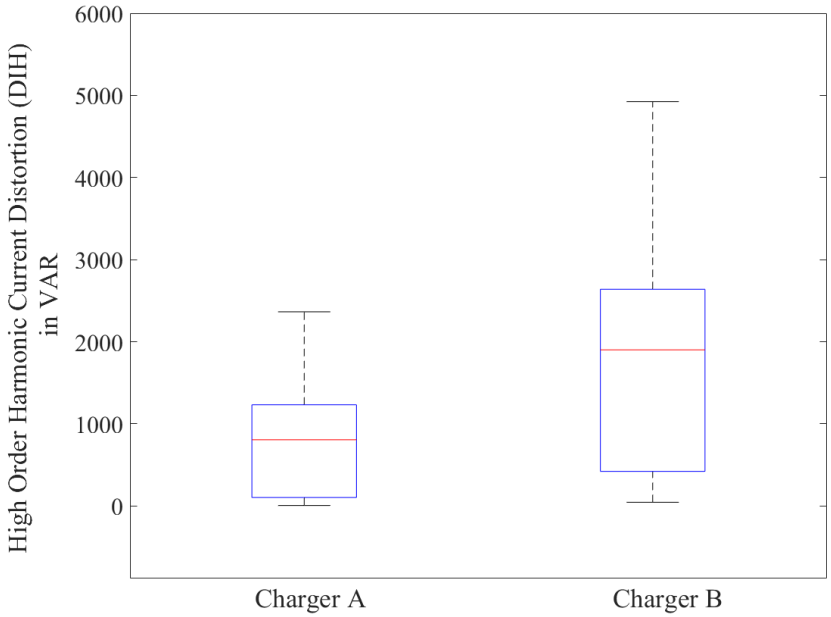

Figure 6.11: High order Harmonic current distortion power

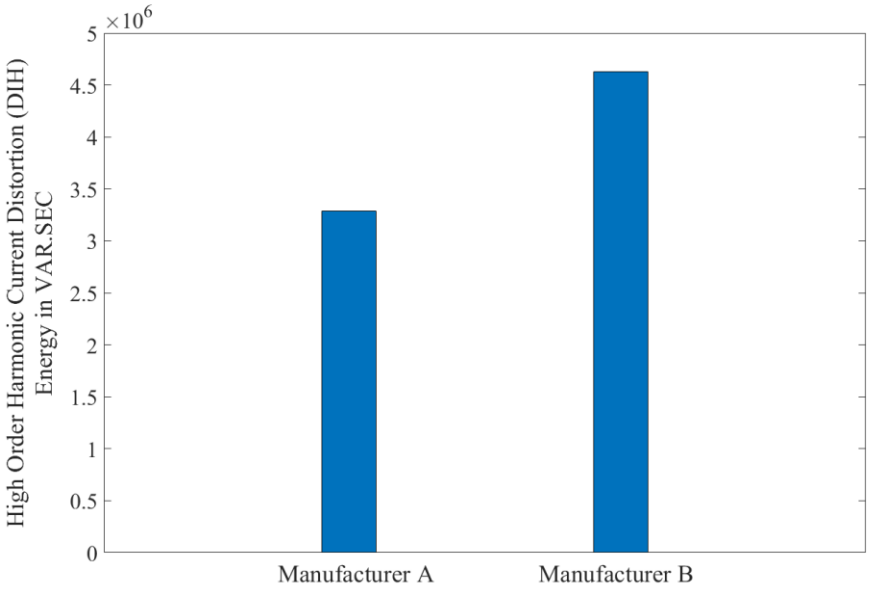

Figure 6.12: High order Harmonic current distortion energy

6.3.3 High-order harmonic current and voltage interference apparent power

Figure 6.13 depicts the high-order harmonic current interference apparent power (S_{eHLH}) and the high order harmonic voltage interference apparent power (S_{eHHL}) in case of both manufacturers A and B chargers. The figure shows in general the high-order harmonic current interference apparent power is higher than the high-order harmonic voltage interference apparent power. Also, the figure reveals the effect of manufacturer B charger in increasing both high-order harmonic interference apparent power (S_{eHLH} and S_{eHHL}) compared to those of manufacturer A charger.

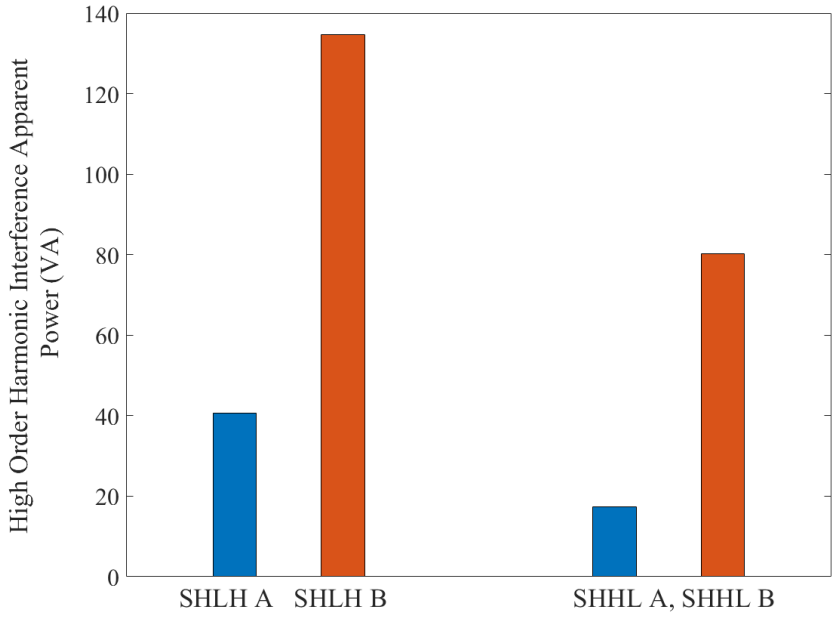

Figure 6.13: High order harmonic interreference apparent power

6.3.4 Low-order and high-order harmonic non-fundamental apparent powers

Table 6.3 lists the mean value of the harmonic non-fundamental apparent powers as a mean to compare the contribution of both chargers.

Table 6.3 Low and high order harmonic non-fundamental apparent power

Apparent Power (VA)	Charger type	
	Manufacturer A	Manufacturer B
S_{eNL}	20,255	33,675
S_{eNH}	822	1,947
S_{eNI}	21	177
S_{eN}	20,272	33,732

In general, the results in table 6.3 clearly show that manufacturer B charger contributes more compared to manufacturer A charger in all non-fundamental apparent power quantities. Specifically, at the high-order harmonics manufacturer B charger contributes

more than double the value of S_{eNH} while in terms of the non-fundamental effective interference apparent power, manufacturer B charger was found to contribute nearly 8 times that of manufacturer A charger. The results also show an overall difference of 13.46 kVA in the non-fundamental apparent power S_{eN}, which represents the vector sum of the three power components (S_{eNl}, S_{eNH} and S_{eNI}), produced by manufacturer B charger.

6.4 Harmonic Pollution Factor (HPF)

The harmonic pollution factor (HPF) is another parameter to calculate the impact of non-linear load as harmonic pollution source to the system, and it's calculated as the percentage of the non-fundamental apparent power to the fundamental apparent power. HPF can be used to quantify the harmonic pollution contribution of the chargers. Visual inspection of figure 6.14 reveals that HPF of manufacturer B charger is measuring 20% while that of manufacturer A charger is measuring only 10%. This clearly shows that HPF of manufacturer B charger is almost double the value of that of manufacturer A charger and therefore the harmonic distortion produced by manufacturer B charger at both low and high-order harmonics significantly increases the non-fundamental apparent power, which was reflected on the harmonic pollution factor.

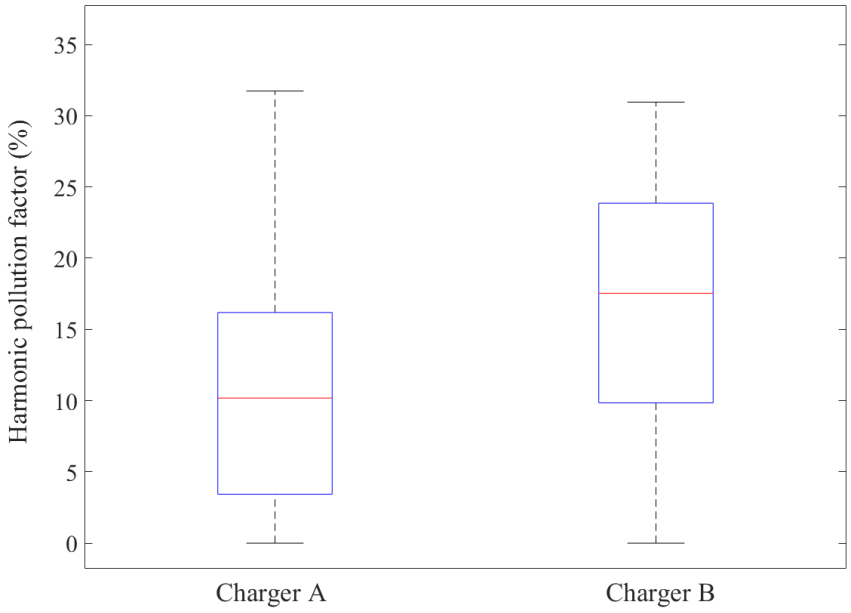

Figure 6.14: Harmonic pollution factor

6.5 Supraharmonics Emission.

Supraharmonics is the harmonic emission occurring within the frequency range 2 to 150 kHz as defined in [17]. To understand the emission of supraharmonics let's consider scenario 2, where charger from manufacturer B is used to charge PEV Chevy Bolt and the charging profile is recorded each 30 second for the charging period. Figure 6.15 shows 3D spectrogram for non-fundamental harmonic current emitted as obtained from the charging profile, where's the (X-axis) represent the time steps, while (Y-axis) is harmonic order up to 124 order, and the (Z-axis) is representing the harmonic current. It can be noticed that the harmonics emission in the harmonic order range are 33-40, 60-70, and 100-120, which can be considered as supraharmonics pollution. Figure 6.16

represents the 2D spectra of charging profile, and again it can be observed the harmonic pollution in supraharmonics range.

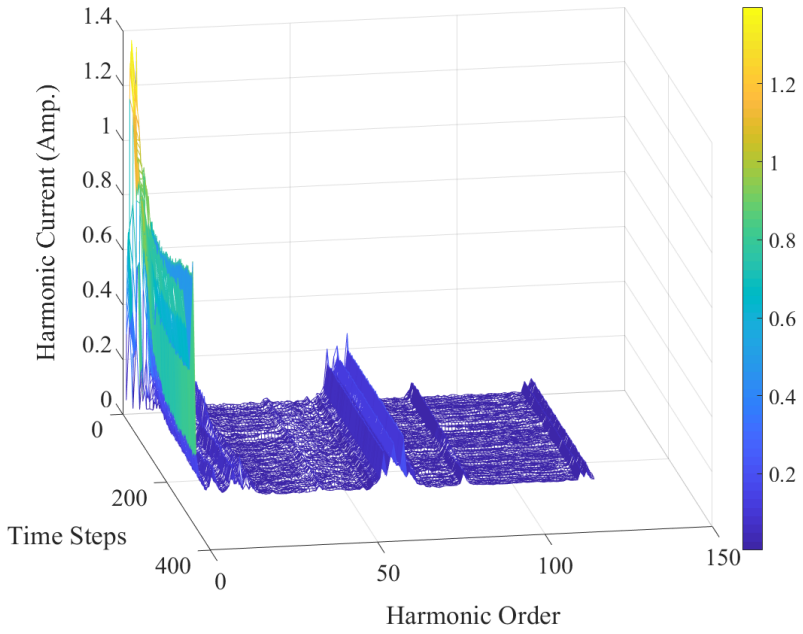

Figure 6.15: 3D Spectrogram of Supraharmonics emission of Chevy Bolt charging from Charger B

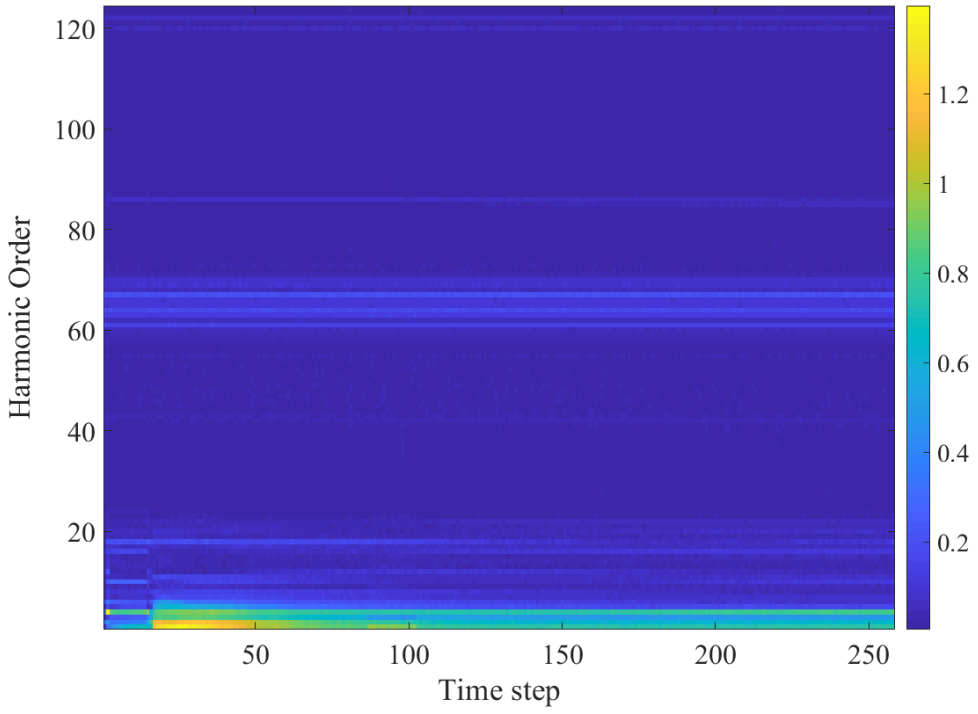

Figure 6.16:2D Spectrogram of Supraharmonics emission of Chevy Bolt charging from Charger B

6.6 Voltage Flicker Measurement.

The IEEE 1453-2004 [30] standard states the planning and the compatibility levels for flickers depends on measurement of flicker at PCC, which is defined as the point on electrical power system electrically closest to a particular fluctuating load. The values 1 and 0.8 are the compatibility limits for P_{st} and P_{lt} respectively while 0.9 and 0.7 are the planning values for P_{st} and P_{lt} respectively.

In this study, the measurements took place in the simulation for IEEE 34 bus system at PCC (bus 16, node 832 figure. 5.3) to eventually measure the effect of the twenty FCS on the rest of the studied system.

The calculated mean of P_{ST} and P_{lt} for the FCS in the case of chargers from manufacturers A and B with charging the three kinds of electrical vehicles is calculated to be 0.86. The value is fixed for all chargers' manufacturers and vehicles' types as it depends on the switching on and off of the high loads connected to the grid. The value indicates violation in P_{lt} value of the acceptable limit in table 3.1. and it shows no violations of the short-term perceptions. Also, it can be summarized that the FCSs have impact on the voltage flickering in long term perception only as it exceeds the acceptable limit, while for short term perception, there are no violation as the value is fallen within the limit. The standard states there are acceptable level of violation to the planning value of P_{st} by one percent, provided that the violation doesn't stay for long time. For example, for 95% probability and given the 1008 P_{st} intervals in a week, a connected load could exceed the recommended P_{st} value for 50 ten-minute intervals and remain within compliance. It is preferred, however, that the 99% probability level be used; thus only 10 P_{st} intervals in a week could be exceeded and compliance maintained. These probability levels are based on cumulative distribution calculations. By setting flicker limits such that the planning levels are exceeded only a small percentage of the time, customer complaints and equipment malfunctions will be minimized. As a general guideline, P_{st} and P_{lt} should not exceed the planning levels more than 1% of the time (99% probability level), with a minimum assessment period of one week. Thus, in our study, the P_{st} value is around one percent of the planning level for more than 12 consecutive time intervals, which leads to P_{lt} value to be higher than the acceptable level by [30].

6.7 Summary

This chapter presents the results of implementing the proposed approach to incorporate the fast charging stations load to the IEEE 34-bus standard test system using a Monte Carlo simulation after modifying it to estimate the charging profile of the FCSs. The arrival distribution of the vehicles to the charging station is considered in order to probabilistic assessment of the electric power quality considering different vehicle types, and chargers' types and vehicles. New power and energy quantities mathematical formula that have been developed and are used in order to compare the impact of chargers from different manufacturers on the power quality of the distribution system with indices of the low order current / voltage distortion power and energy and the interference power resulting of the interactions between the low order or high order current or voltage distortions. The results show that fast charging stations from one manufacturer has the most significant harmonic distortion in low and high order harmonics on system level. The comparison of the results is presented in this chapter between different chargers' manufacturers as well as different vehicles' types.

Chapter 7. Conclusions and Recommendations

7.1 Conclusions

This thesis studies the effect of integrating large-scale high-power fast charging stations on the power quality in the primary distribution system in terms of low-order and high-order harmonics, supraharmonics and voltage flickers at both the fast charging stations level and at system level. The high-power fast chargers from different manufacturers installed in fast charging stations are considered in this study as well as different make of plug in electric vehicles are also considered. In this work, a probabilistic model of fast charging stations level 3 is developed. In order to address the uncertainties associated with the integration of electric vehicles charging profile into the distribution system such as battery state of charge and the arrival time of the plug-in electric vehicles, a Monte Carlo simulation is used to estimate such impact on the distribution system. The mathematical formulation of the effective distortion and apparent power in three-phase systems are presented and are then used to quantify the harmonic distortion at both the low-order and the high-order harmonic distortion.

At the system level, the results have shown that chargers from different manufacturers may inject different levels of harmonic distortions on both the low-order and high-order harmonics that can reach 18%. Furthermore, the chargers from different manufacturers may have different frequency contents at both the low-order and high-order harmonics. The frequency contents of chargers from one manufacturer are sporadic at the low-order harmonics while the frequency contents of chargers from another manufacturer are concentrated at the high-order harmonics. The different levels of the harmonic distortion contribution of the fast chargers is mainly influencing the harmonic distortion power,

the non-fundamental apparent power and the harmonic interference apparent power. The results have shown that the harmonic contribution of chargers from one manufacturer can be double that of another manufacturer in case of high-order harmonic non-fundamental apparent power and one and a half in case of the low-order harmonic non-fundamental apparent power. On the other hand, the contribution of the chargers to the non-fundamental interference apparent power was found to reach 8 times that of another charger from different manufacturer, which demonstrates the large difference in the harmonic pollution emitted from these chargers that can reach up to 20% in terms of the harmonic pollution factor.

The following concludes the main findings of the work presented in this thesis:

- Increasing the number of FCSs has a clear effect on violating the harmonic distortion limits recommended (%5).
- The chargers from different manufacturers may inject different levels of harmonic distortion in the low and high frequency range.
- The frequency contents of the chargers from one manufacturer are concentrated at low-order harmonics while the frequency contents of the chargers from another manufacturer are sporadic at high-order harmonics.
- The harmonic contribution of the chargers from one manufacturer can be double that of another manufacturer.
- Different types of electrical vehicle may have different level of harmonics injection on system.
- The charger type has the most significant impact as the harmonic distortion source on the electrical system, rather than the vehicle types.

- Supraharmonics can be identified with the FCSs at high level of frequency, and chargers from different manufacturer can react differently as a source of harmonics in supraharmonics frequency range.
- The long-term flicker severity index values violate the borderline of standard flicker level while in short term perception was found to be within the acceptable range.

The contribution of this thesis can be summarized in the followings:

- Development of new three-phases power and energy quantities to assess the impact of the charging in low order and high order harmonics range and study the interaction between them so that helps to choose the right mitigation technique.
- Quantification of the impact of integrating large-scale of fast charging stations at both the station level and at the distribution system level.

Comparison between the impacts of the fast charging stations' manufacturers at system level as well as different vehicles' manufacturers.

Long term prediction for large-scale fast charging stations connected to the power distribution system.

7.2 Recommendations

Following the analysis performed in this work, a set of recommendations is appropriate. Considering what has been seen in the analysis of this thesis, the distribution system must respond to the predicted harmonics, supraharmonics and voltage fluctuations caused by increasing the number of fast charging stations. Given the work performed in this thesis, and the results outcome from the simulation, further action followed up to be done properly 1) At the fast charging stations level: Standards have to be developed

for manufacturers of the chargers to eliminate the emission of the harmonic distortion from the chargers by some mitigation techniques to reach a certain limit of harmonic distortion before its approved to be install to the electrical power grid. 2) At the system level: Considering emission on the low order and high order harmonic distortion, Utilities must strategically locate harmonic mitigation devices such as filters in location depends on the harmonic distortion measurements, to reduce harmonic distortion to be within the allowable range of low order and high order harmonics.

Besides, The IEEE 519-2014 standards need to be extended to include the new power quantities equations to separate the low order and high order harmonic distortion power due to current and voltage low and high order harmonics distortions, as well as the interference power that resulting from interaction between low order and high order current/ voltage harmonic distortions.

7.3 Future Work

Some next steps that can be taken to build on the work presented in this thesis are:

At the charger level: investigating the effect of more manufacturers for the fast charging stations. Besides, measurements can be done from chargers connected to the power grid directly without batteries and inventers connected. Which will cause more harmonic distortion from and to the power system.

At simulation level: Different vehicles from different manufacturers as well as different manufacturers for the charging station need to be probabilistically estimated each hours to reach closer approach. Each of these additions will allow the proposed technique to be more realistic in a home environment.

REFERENCES

[1] "There are over 23,620 EVs in Canada and only 5,841 charging stations," *MobileSyrup*, 08-Jan-2019. [Online]. Available: https://mobilesyrup.com/2019/01/08/canada-electirc-vehicle-statistics-ev-canada/. [Accessed: 31-Jan-2020].

[2] "42 new charging stations added to downtown Calgary parkades," *Global News*. [Online]. Available: https://globalnews.ca/news/5207097/calgary-electric-vehicle-charging-stations-parkade/. [Accessed: 18-Jan-2020].

[3] "Petro-Canada installing 50 fast-charging EV stations across the country — but is there demand?," *Global News*. [Online]. Available: https://globalnews.ca/news/4976930/petro-canada-fast-charging-electric-vehicle-stations/. [Accessed: 18-Jan-2020].

[4] "GPI_DCFC_Analysis_July_2019.pdf." .

[5] "Electric Vehicle Charging Stations : Technical Installation Guide," p. 52.

[6] "BC-DCFC-Gap-Analysis-Report-FBC_Aug-2015.pdf." .

[7] C. N. · P. Jul 18, 2019 2:49 PM ET | Last Updated: July 18, and 2019, "Cross-country by electric vehicle may soon be an easier trip for northerners, advocate says | CBC News," *CBC*, 18-Jul-2019. [Online]. Available: https://www.cbc.ca/news/canada/sudbury/electric-vehicle-northern-ontario-1.5216441. [Accessed: 20-Jan-2020].

[8] "Public charging station," *vehiculeselectriques.gouv.qc.ca*. [Online]. Available: http://vehiculeselectriques.gouv.qc.ca/english/decouvrir/recharge/recharge-publique.asp. [Accessed: 20-Jan-2020].

[9] S. K. Rönnberg, A. Gil-De-Castro, and R. Medina-Gracia, "Supraharmonics in European and North American Low-Voltage Networks," in *2018 IEEE International Conference on Environment and Electrical Engineering and 2018 IEEE Industrial and Commercial Power Systems Europe (EEEIC / I CPS Europe)*, 2018, pp. 1–6, doi: 10.1109/EEEIC.2018.8493930.

[10] "IEEE Recommended Practice and Requirements for Harmonic Control in Electric Power Systems," *IEEE Std 519-2014 (Revision of IEEE Std 519-1992)*, pp. 1–29, Jun. 2014, doi: 10.1109/IEEESTD.2014.6826459.

[11] S. M. Alshareef and W. G. Morsi, "Impact of fast charging stations on the voltage flicker in the electric power distribution systems," in *2017 IEEE Electrical Power and Energy Conference (EPEC)*, 2017, pp. 1–6, doi: 10.1109/EPEC.2017.8286226.

[12] A. Lucas, F. Bonavitacola, E. Kotsakis, and G. Fulli, "Grid harmonic impact of multiple electric vehicle fast charging," *Electric Power Systems Research*, vol. 127, pp. 13–21, Oct. 2015, doi: 10.1016/j.epsr.2015.05.012.

[13] "IEC 61000-3-12, Electromagnetic compatibility (EMC) – Part 3-12: Limits – Limits for harmonic currents produced by equipment connected to public low-voltage systems with input current >16 A and İ75 A per phase, (2011)." .

[14] "IEC, IEC 61000-2-4, Electromagnetic compatibility (EMC)-Part 2-4: Environment-compatibility Levels in Industrial Plants for Low-frequency Conducted Disturbances, (2014)." .

[15] “propagation-of-supraharmonics-in-the-low-voltage-grid-energiforskrapport-2017-461.pdf.” .
[16] S. K. Rönnberg, A. G. Castro, M. H. J. Bollen, A. Moreno-Munoz, and E. Romero-Cadaval, “Supraharmonics from power electronics converters,” in *2015 9th International Conference on Compatibility and Power Electronics (CPE)*, 2015, pp. 539–544, doi: 10.1109/CPE.2015.7231133.
[17] A. Moreno-Munoz, A. Gil-de-Castro, E. Romero-Cavadal, S. Rönnberg, and M. Bollen, “Supraharmonics (2 to 150 kHz) and multi-level converters,” in *2015 IEEE 5th International Conference on Power Engineering, Energy and Electrical Drives (POWERENG)*, 2015, pp. 37–41, doi: 10.1109/PowerEng.2015.7266293.
[18] Aiqiang Pan, Yongwei Zhu, Lijia Ren, Tiantian Chen, Sun Wen, and Wang Yun, “Harmonic research of electric vehicle fast chargers,” in *2016 IEEE PES Asia-Pacific Power and Energy Engineering Conference (APPEEC)*, 2016, pp. 2545–2549, doi: 10.1109/APPEEC.2016.7779947.
[19] Y. Sun, E. De Jong, V. Cuk, and J. F. G. Cobben, “Ultra fast charging station harmonic resonance analysis in the Dutch MV grid: application of power converter harmonic model,” *CIRED - Open Access Proceedings Journal*, vol. 2017, no. 1, pp. 879–882, 2017, doi: 10.1049/oap-cired.2017.1074.
[20] Y. Sun, E. C. W. de Jong, V. Cuk, and J. F. G. Cobben, “Harmonic resonance risk of massive ultra fast charging station grid integration,” in *2018 18th International Conference on Harmonics and Quality of Power (ICHQP)*, 2018, pp. 1–6, doi: 10.1109/ICHQP.2018.8378897.
[21] T. Fujun, X. Ruiheng, C. Dong, R. Lijia, Y. Quanning, and Z. Yan, “Research on the harmonic characteristics of electric vehicle fast charging stations,” in *2017 2nd International Conference on Power and Renewable Energy (ICPRE)*, 2017, pp. 805–809, doi: 10.1109/ICPRE.2017.8390645.
[22] L. Cheng, B. Wu, H. Chen, W. Ma, and G. Zhang, “Load Forecasting and Harmonic Analysis for EV Charging Station,” in *2018 IEEE Innovative Smart Grid Technologies - Asia (ISGT Asia)*, 2018, pp. 139–144, doi: 10.1109/ISGT-Asia.2018.8467908.
[23] T. Pothinun and S. Premrudeepreechacharn, “Power Quality Impact of Charging Station on MV Distribution Networks: A Case Study in PEA Electrical Power System,” in *2018 53rd International Universities Power Engineering Conference (UPEC)*, 2018, pp. 1–6, doi: 10.1109/UPEC.2018.8541921.
[24] R. Torquato, F. C. L. Trindade, W. Freitas, G. R. T. Hax, and V. T. Arioli, “Comparative study of the harmonic impact of different plug-in electric vehicles and charging stations — A Brazilian case study,” in *2016 17th International Conference on Harmonics and Quality of Power (ICHQP)*, 2016, pp. 611–616, doi: 10.1109/ICHQP.2016.7783433.
[25] J. Meyer, S. Mueller, S. Ungethuem, X. Xiao, A. Collin, and S. Djokic, “Harmonic and supraharmonic emission of on-board electric vehicle chargers,” in *2016 IEEE PES Transmission Distribution Conference and Exposition-Latin America (PES T D-LA)*, 2016, pp. 1–7, doi: 10.1109/TDC-LA.2016.7805641.
[26] “Quick_Guide_to_Fast_Charging.pdf.” [online] available https://www.chargepoint.com/files/Quick_Guide_to_Fast_Charging.pdf .
[27] A. Hajimiragha, C. A. Canizares, M. W. Fowler, and A. Elkamel, “Optimal Transition to Plug-In Hybrid Electric Vehicles in Ontario, Canada, Considering the

Electricity-Grid Limitations," *IEEE Transactions on Industrial Electronics*, vol. 57, no. 2, pp. 690–701, Feb. 2010, doi: 10.1109/TIE.2009.2025711.
[28] "Voltage Fluctuation and Lamp Flicker Establishment Of Guidelines, Pennsylvania Power & Light December 1994." .
[29] "IEC 60050, International Electrotechnical Vocabulary, Details for IEV number 161-08-13: 'flicker.' [online]. Available: http://www.electropedia.org/iev/iev.nsf/display?openform&ievref=161-08-13." .
[30] "IEEE Recommended Practice for Measurement and Limits of Voltage Fluctuations and Associated Light Flicker on AC Power Systems," *IEEE Std 1453-2004 (Adoption of CEI/IEC 61000-4-15:1997+A1:2003)*, pp. 1–74, Mar. 2005, doi: 10.1109/IEEESTD.2005.95938.
[31] "IEEE Standard Definitions for the Measurement of Electric Power Quantities Under Sinusoidal, Nonsinusoidal, Balanced, or Unbalanced Conditions," *IEEE Std 1459-2010 (Revision of IEEE Std 1459-2000)*, pp. 1–50, Mar. 2010, doi: 10.1109/IEEESTD.2010.5439063.
[32] M. K. Gray and W. G. Morsi, "Power Quality Assessment in Distribution Systems Embedded With Plug-In Hybrid and Battery Electric Vehicles," *IEEE Trans. Power Syst.*, vol. 30, no. 2, pp. 663–671, Mar. 2015, doi: 10.1109/TPWRS.2014.2332058.
[33] K. O'Connell, "Heating Effects Through Harmonic Distortion on Electric Cables in the Built Environment," 2013, doi: 10.21427/D7X310.
[34] "Power_Quality_Reference_Guide.pdf." [online] available. https://www.bchydro.com/content/dam/BCHydro/customer-portal/documents/power-smart/business/programs/power-quality-reference-guide.pdf.
[35] "PX5-UsersGuide-RevJ.pdf." [online] available. https://www.dranetz.com/wp-content/uploads/2014/02/PX5-UsersGuide-RevJ.pdf
[36] K. P. Schneider *et al.*, "Analytic Considerations and Design Basis for the IEEE Distribution Test Feeders," *IEEE Transactions on Power Systems*, vol. 33, no. 3, pp. 3181–3188, May 2018, doi: 10.1109/TPWRS.2017.2760011.
[37] "Resources | PES Test Feeder." [Online]. Available: https://site.ieee.org/pes-testfeeders/resources/. [Accessed: 21-Jan-2020].
[38] K. Yunus, H. Z. De La Parra, and M. Reza, "Distribution grid impact of Plug-In Electric Vehicles charging at fast charging stations using stochastic charging model," in *Proceedings of the 2011 14th European Conference on Power Electronics and Applications*, 2011, pp. 1–11.

APPENDICES

Appendix A.

IEEE 34 Node Test Feeder

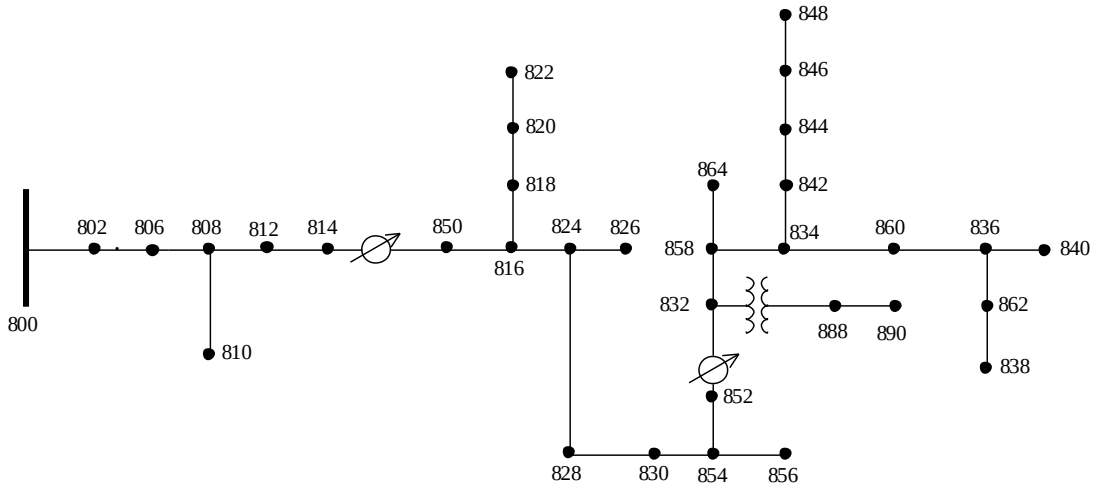

Overhead Line Configurations (Config.)

Config.	Phasing	Phase ACSR	Neutral ACSR	Spacing ID
300	B A C N	1/0	1/0	500
301	B A C N	#2 6/1	#2 6/1	500
302	A N	#4 6/1	#4 6/1	510
303	B N	#4 6/1	#4 6/1	510
304	B N	#2 6/1	#2 6/1	510

Line Segment Data

Node A	Node B	Length(ft.)	Config.
800	802	2580	300
802	806	1730	300
806	808	32230	300
808	810	5804	303
808	812	37500	300
812	814	29730	300
814	850	10	301
816	818	1710	302
816	824	10210	301
818	820	48150	302
820	822	13740	302
824	826	3030	303
824	828	840	301
828	830	20440	301
830	854	520	301
832	858	4900	301
832	888	0	XFM-1
834	860	2020	301
834	842	280	301
836	840	860	301
836	862	280	301
842	844	1350	301
844	846	3640	301
846	848	530	301
850	816	310	301
852	832	10	301
854	856	23330	303
854	852	36830	301
858	864	1620	302
858	834	5830	301
860	836	2680	301
862	838	4860	304
888	890	10560	300

Transformer Data

	kVA	kV-high	kV-low	R - %	X - %
Substation:	2500	69 - D	24.9 -Gr. W	1	8
XFM -1	500	24.9 - Gr.W	4.16 - Gr. W	1.9	4.08

Spot Loads

Node	Load Model	Ph-1 kW	Ph-1 kVAr	Ph-2 kW	Ph-2 kVAr	Ph-3 kW	Ph-4 kVAr
860	Y-PQ	20	16	20	16	20	16
840	Y-I	9	7	9	7	9	7
844	Y-Z	135	105	135	105	135	105
848	D-PQ	20	16	20	16	20	16
890	D-I	150	75	150	75	150	75
830	D-Z	10	5	10	5	25	10
Total		344	224	344	224	359	229

Distributed Loads

Node A	Node B	Load Model	Ph-1 kW	Ph-1 kVAr	Ph-2 kW	Ph-2 kVAr	Ph-3 kW	Ph-3 kVAr
802	806	Y-PQ	0	0	30	15	25	14
808	810	Y-I	0	0	16	8	0	0
818	820	Y-Z	34	17	0	0	0	0
820	822	Y-PQ	135	70	0	0	0	0
816	824	D-I	0	0	5	2	0	0
824	826	Y-I	0	0	40	20	0	0
824	828	Y-PQ	0	0	0	0	4	2
828	830	Y-PQ	7	3	0	0	0	0
854	856	Y-PQ	0	0	4	2	0	0
832	858	D-Z	7	3	2	1	6	3
858	864	Y-PQ	2	1	0	0	0	0
858	834	D-PQ	4	2	15	8	13	7
834	860	D-Z	16	8	20	10	110	55
860	836	D-PQ	30	15	10	6	42	22
836	840	D-I	18	9	22	11	0	0
862	838	Y-PQ	0	0	28	14	0	0
842	844	Y-PQ	9	5	0	0	0	0
844	846	Y-PQ	0	0	25	12	20	11
846	848	Y-PQ	0	0	23	11	0	0
Total			262	133	240	120	220	114

Shunt Capacitors

Node	Ph-A kVAr	Ph-B kVAr	Ph-C kVAr
844	100	100	100
848	150	150	150
Total	250	250	250

Regulator Data

Regulator ID:	1		
Line Segment:	814 - 850		
Location:	814		
Phases:	A - B -C		
Connection:	3-Ph,LG		
Monitoring Phase:	A-B-C		
Bandwidth:	2.0 volts		
PT Ratio:	120		
Primary CT Rating:	100		
Compensator Settings:	Ph-A	Ph-B	Ph-C
R - Setting:	2.7	2.7	2.7
X - Setting:	1.6	1.6	1.6
Volltage Level:	122	122	122

Regulator ID:	2		
Line Segment:	852 - 832		
Location:	852		
Phases:	A - B -C		
Connection:	3-Ph,LG		
Monitoring Phase:	A-B-C		
Bandwidth:	2.0 volts		
PT Ratio:	120		
Primary CT Rating:	100		
Compensator Settings:	Ph-A	Ph-B	Ph-C
R - Setting:	2.5	2.5	2.5
X - Setting:	1.5	1.5	1.5
Volltage Level:	124	124	124

IEEE 34 Node Test Feeder

Impedances

```
Configuration 300:

--------- Z & B Matrices Before Changes ---------

           Z (R +jX) in ohms per mile
 1.3368  1.3343   0.2101  0.5779   0.2130  0.5015
                  1.3238  1.3569   0.2066  0.4591
                                   1.3294  1.3471
          B in micro Siemens per mile
            5.3350   -1.5313   -0.9943
                      5.0979   -0.6212
                                4.8880
Configuration 301:

           Z (R +jX) in ohms per mile
 1.9300  1.4115   0.2327  0.6442   0.2359  0.5691
                  1.9157  1.4281   0.2288  0.5238
                                   1.9219  1.4209
          B in micro Siemens per mile
            5.1207   -1.4364   -0.9402
                      4.9055   -0.5951
                                4.7154

Configuration 302:

           Z (R +jX) in ohms per mile
 2.7995  1.4855   0.0000  0.0000   0.0000  0.0000
```

```
                  0.0000  0.0000   0.0000  0.0000
                                   0.0000  0.0000
          B in micro Siemens per mile
            4.2251    0.0000    0.0000
                      0.0000    0.0000
                                0.0000
```

Configuration 303:

```
           Z (R +jX) in ohms per mile
 0.0000  0.0000   0.0000  0.0000   0.0000  0.0000
                  2.7995  1.4855   0.0000  0.0000
                                   0.0000  0.0000
          B in micro Siemens per mile
            0.0000    0.0000    0.0000
                      4.2251    0.0000
                                0.0000
```

Configuration 304:

```
          Z (R +jX) in ohms per mile
0.0000  0.0000   0.0000  0.0000   0.0000  0.0000
                 1.9217  1.4212   0.0000  0.0000
                                  0.0000  0.0000
         B in micro Siemens per mile
           0.0000    0.0000    0.0000
                     4.3637    0.0000
                               0.0000
```

Power Flow Results

```
- R A D I A L   F L O W   S U M M A R Y - DATE:  6-24-2004 AT 16:34:11 HOURS ---
 SUBSTATION:  IEEE 34;   FEEDER:  IEEE 34
 ------------------------------------------------------------------------------
-
 SYSTEM        PHASE             PHASE             PHASE             TOTAL
 INPUT -------(A)-------|-------(B)-------|-------(C)-------|------------------
 kW   :       759.136   |       666.663   |       617.072   |      2042.872
 kVAr :       171.727   |        90.137   |        28.394   |       290.258
 kVA  :       778.318   |       672.729   |       617.725   |      2063.389
 PF   :        .9754    |        .9910    |        .9989    |        .9901

 LOAD  --(A-N)----(A-B)-|--(B-N)----(B-C)-|--(C-N)----(C-A)-|---WYE-----DELTA--
 kW   :   359.9    246.4|   339.3    243.3|   221.8    359.0|   921.0    848.8
  TOT :       606.322   |       582.662   |       580.840   |      1769.824
                        |                 |                 |
 kVAr :   230.9    128.7|   216.9    128.7|   161.8    184.6|   609.6    441.9
  TOT :       359.531   |       345.609   |       346.407   |      1051.547
                        |                 |                 |
 kVA  :   427.6    278.0|   402.7    275.3|   274.6    403.7|  1104.5    957.0
  TOT :       704.903   |       677.452   |       676.293   |      2058.647
                        |                 |                 |
 PF   :   .8417    .8864|   .8425    .8840|   .8078    .8894|   .8339    .8870
  TOT :        .8601    |        .8601    |        .8589    |        .8597

 LOSSES ------(A)-------|-------(B)-------|-------(C)-------|------------------
 kW   :       114.836   |        80.389   |        77.824   |       273.049
 kVAr :        14.200   |        10.989   |         9.810   |        34.999
 kVA  :       115.711   |        81.137   |        78.440   |       275.283

 CAPAC --(A-N)----(A-B)-|--(B-N)----(B-C)-|--(C-N)----(C-A)-|---WYE-----DELTA--
 R-kVA:   250.0       .0|   250.0       .0|   250.0       .0|   750.0       .0
  TOT :       250.000   |       250.000   |       250.000   |       750.000
                        |                 |                 |
 A-kVA:   265.7       .0|   264.8       .0|   265.9       .0|   796.3       .0
  TOT :       265.658   |       264.760   |       265.869   |        796.287
```

--- **V O L T A G E P R O F I L E** ---- DATE: 6-24-2004 AT 16:34:18 HOURS ----
SUBSTATION: IEEE 34; FEEDER: IEEE 34

NODE	MAG ANGLE	MAG ANGLE	MAG ANGLE	mi.to SR
	A-N	B-N	C-N	
800	1.0500 at .00	1.0500 at -120.00	1.0500 at 120.00	.000
802	1.0475 at -.05	1.0484 at -120.07	1.0484 at 119.95	.489
806	1.0457 at -.08	1.0474 at -120.11	1.0474 at 119.92	.816
808	1.0136 at -.75	1.0296 at -120.95	1.0289 at 119.30	6.920
810		1.0294 at -120.95		8.020
812	.9763 at -1.57	1.0100 at -121.92	1.0069 at 118.59	14.023
814	.9467 at -2.26	.9945 at -122.70	.9893 at 118.01	19.653
RG10	1.0177 at -2.26	1.0255 at -122.70	1.0203 at 118.01	19.654
850	1.0176 at -2.26	1.0255 at -122.70	1.0203 at 118.01	19.655
816	1.0172 at -2.26	1.0253 at -122.71	1.0200 at 118.01	19.714
818	1.0163 at -2.27			20.038
820	.9926 at -2.32			29.157
822	.9895 at -2.33			31.760
824	1.0082 at -2.37	1.0158 at -122.94	1.0116 at 117.76	21.648
826		1.0156 at -122.94		22.222
828	1.0074 at -2.38	1.0151 at -122.95	1.0109 at 117.75	21.807
830	.9894 at -2.63	.9982 at -123.39	.9938 at 117.25	25.678
854	.9890 at -2.64	.9978 at -123.40	.9934 at 117.24	25.777
852	.9581 at -3.11	.9680 at -124.18	.9637 at 116.33	32.752
RG11	1.0359 at -3.11	1.0345 at -124.18	1.0360 at 116.33	32.752
832	1.0359 at -3.11	1.0345 at -124.18	1.0360 at 116.33	32.754
858	1.0336 at -3.17	1.0322 at -124.28	1.0338 at 116.22	33.682
834	1.0309 at -3.24	1.0295 at -124.39	1.0313 at 116.09	34.786
842	1.0309 at -3.25	1.0294 at -124.39	1.0313 at 116.09	34.839
844	1.0307 at -3.27	1.0291 at -124.42	1.0311 at 116.06	35.095
846	1.0309 at -3.32	1.0291 at -124.46	1.0313 at 116.01	35.784
848	1.0310 at -3.32	1.0291 at -124.47	1.0314 at 116.00	35.885
860	1.0305 at -3.24	1.0291 at -124.39	1.0310 at 116.09	35.169
836	1.0303 at -3.23	1.0287 at -124.39	1.0308 at 116.09	35.677
840	1.0303 at -3.23	1.0287 at -124.39	1.0308 at 116.09	35.839
862	1.0303 at -3.23	1.0287 at -124.39	1.0308 at 116.09	35.730
838		1.0285 at -124.39		36.650
864	1.0336 at -3.17			33.989
XF10	.9997 at -4.63	.9983 at -125.73	1.0000 at 114.82	32.754
888	.9996 at -4.64	.9983 at -125.73	1.0000 at 114.82	32.754
890	.9167 at -5.19	.9235 at -126.78	.9177 at 113.98	34.754
856		.9977 at -123.41		30.195

---------- **VOLTAGE REGULATOR DATA** ---- DATE: 6-24-2004 AT 16:34:22 HOURS --
SUBSTATION: IEEE 34; FEEDER: IEEE 34

[NODE]	[VREG]	[SEG]	[NODE]	MODEL	OPT	BNDW
814	RG10	850	850	Phase A & B & C, Wye	RX	2.00

PHASE	LDCTR	VOLT HOLD	R-VOLT	X-VOLT	PT RATIO	CT RATE	TAP
1		122.000	2.700	1.600	120.00	100.00	12
2		122.000	2.700	1.600	120.00	100.00	5
3		122.000	2.700	1.600	120.00	100.00	5

[NODE]	[VREG]	[SEG]	[NODE]	MODEL	OPT	BNDW
852	RG11	832	832	Phase A & B & C, Wye	RX	2.00

PHASE	LDCTR	VOLT HOLD	R-VOLT	X-VOLT	PT RATIO	CT RATE	TAP
1		124.000	2.500	1.500	120.00	100.00	13
2		124.000	2.500	1.500	120.00	100.00	11
3		124.000	2.500	1.500	120.00	100.00	12

```
- R A D I A L   P O W E R   F L O W  ---  DATE:  6-24-2004 AT 16:34:32 HOURS ---
 SUBSTATION:  IEEE 34;   FEEDER:  IEEE 34
 ------------------------------------------------------------------------------
    NODE      VALUE         PHASE A         PHASE B         PHASE C     UNT O/L<
                            (LINE A)        (LINE B)        (LINE C)        60.%
 ---------------------*--------A-------*-------B-------*-------C-------*--------
 NODE: 800       VOLTS:   1.050     .00   1.050 -120.00   1.050  120.00 MAG/ANG
 kVll  24.900           NO LOAD OR CAPACITOR REPRESENTED AT SOURCE NODE

 TO NODE 802   .......:   51.56  -12.74   44.57 -127.70   40.92  117.37 AMP/DG
 <802   > LOSS=  3.472:    (  1.637)       (   .978)       (   .858)    kW
 ---------------------*--------A-------*-------B-------*-------C-------*--------
 NODE: 802       VOLTS:   1.047    -.05   1.048 -120.07   1.048  119.95 MAG/ANG
                   -LD:     .00     .00     .00     .00     .00     .00 kW/kVR
 kVll  24.900      CAP:             .00             .00             .00 kVR

 FROM NODE 800   .....:   51.58  -12.80   44.57 -127.76   40.93  117.31 AMP/DG
 <802   > LOSS=  3.472:    (  1.637)       (   .978)       (   .858)    kW
 TO NODE 806   .......:   51.58  -12.80   44.57 -127.76   40.93  117.31 AMP/DG
 <806   > LOSS=  2.272:    (  1.102)       (   .618)       (   .552)    kW
 ---------------------*--------A-------*-------B-------*-------C-------*--------
 NODE: 806       VOLTS:   1.046    -.08   1.047 -120.11   1.047  119.92 MAG/ANG
                   -LD:     .00     .00     .00     .00     .00     .00 kW/kVR
 kVll  24.900      CAP:             .00             .00             .00 kVR

 FROM NODE 802   .....:   51.59  -12.83   42.47 -126.83   39.24  118.52 AMP/DG
 <806   > LOSS=  2.272:    (  1.102)       (   .618)       (   .552)    kW
 TO NODE 808   .......:   51.59  -12.83   42.47 -126.83   39.24  118.52 AMP/DG
 <808   > LOSS= 41.339:    ( 20.677)       ( 10.780)       (  9.882)    kW
 ---------------------*--------A-------*-------B-------*-------C-------*--------
 NODE: 808       VOLTS:   1.014    -.75   1.030 -120.95   1.029  119.30 MAG/ANG
                   -LD:     .00     .00     .00     .00     .00     .00 kW/kVR
 kVll  24.900      CAP:             .00             .00             .00 kVR

 FROM NODE 806   .....:   51.76  -13.47   42.46 -127.59   39.28  117.76 AMP/DG
 <808   > LOSS= 41.339:    ( 20.677)       ( 10.780)       (  9.882)    kW
 TO NODE 810   .......:                    1.22 -144.62                 AMP/DG
 <810   > LOSS=   .002:                    (   .002)                    kW
 TO NODE 812   .......:   51.76  -13.47   41.30 -127.10   39.28  117.76 AMP/DG
 <812   > LOSS= 47.531:    ( 24.126)       ( 11.644)       ( 11.761)    kW
 ---------------------*--------A-------*-------B-------*-------C-------*--------
 NODE: 810       VOLTS:                   1.029 -120.95                 MAG/ANG
                   -LD:                     .00     .00                 kW/kVR
 kVll  24.900      CAP:                             .00                 kVR

 FROM NODE 808   .....:                     .00     .00                 AMP/DG
 <810   > LOSS=   .002:                    (   .002)                    kW
```

```
- R A D I A L   P O W E R   F L O W  ---  DATE:  6-24-2004 AT 16:34:32 HOURS ---
 SUBSTATION:  IEEE 34;   FEEDER:  IEEE 34
 ------------------------------------------------------------------------------
    NODE      VALUE         PHASE A         PHASE B         PHASE C     UNT O/L<
                            (LINE A)        (LINE B)        (LINE C)        60.%
 ---------------------*--------A-------*-------B-------*-------C-------*--------
 NODE: 812       VOLTS:    .976   -1.57   1.010 -121.92   1.007  118.59 MAG/ANG
                   -LD:     .00     .00     .00     .00     .00     .00 kW/kVR
 kVll  24.900      CAP:             .00             .00             .00 kVR

 FROM NODE 808   .....:   51.95  -14.18   41.29 -127.99   39.33  116.90 AMP/DG
 <812   > LOSS= 47.531:    ( 24.126)       ( 11.644)       ( 11.761)    kW
 TO NODE 814   .......:   51.95  -14.18   41.29 -127.99   39.33  116.90 AMP/DG
 <814   > LOSS= 37.790:    ( 19.245)       (  9.140)       (  9.404)    kW
 ---------------------*--------A-------*-------B-------*-------C-------*--------
 NODE: 814       VOLTS:    .947   -2.26    .994 -122.70    .989  118.01 MAG/ANG
                   -LD:     .00     .00     .00     .00     .00     .00 kW/kVR
 kVll  24.900      CAP:             .00             .00             .00 kVR

 FROM NODE 812   .....:   52.10  -14.73   41.29 -128.69   39.37  116.23 AMP/DG
 <814   > LOSS= 37.790:    ( 19.245)       (  9.140)       (  9.404)    kW
 TO NODE RG10  .<VRG>.:   52.10  -14.73   41.29 -128.69   39.37  116.23 AMP/DG
 <RG10  > LOSS=   .000:    (   .000)       (   .000)       (   .000)    kW
 ---------------------*--------A-------*-------B-------*-------C-------*--------
 NODE: RG10      VOLTS:   1.018   -2.26   1.026 -122.70   1.020  118.01 MAG/ANG
                   -LD:     .00     .00     .00     .00     .00     .00 kW/kVR
 kVll  24.900      CAP:             .00             .00             .00 kVR

 FROM NODE 814   <VRG>:   48.47  -14.73   40.04 -128.69   38.17  116.23 AMP/DG
 <RG10  > LOSS=   .000:    (   .000)       (   .000)       (   .000)    kW
 TO NODE 850   .......:   48.47  -14.73   40.04 -128.69   38.17  116.23 AMP/DG
 <850   > LOSS=   .017:    (   .008)       (   .005)       (   .005)    kW
 ---------------------*--------A-------*-------B-------*-------C-------*--------
 NODE: 850       VOLTS:   1.018   -2.26   1.026 -122.70   1.020  118.01 MAG/ANG
                   -LD:     .00     .00     .00     .00     .00     .00 kW/kVR
 kVll  24.900      CAP:             .00             .00             .00 kVR

 FROM NODE RG10  .....:   48.47  -14.73   40.04 -128.69   38.17  116.23 AMP/DG
 <850   > LOSS=   .017:    (   .008)       (   .005)       (   .005)    kW
 TO NODE 816   .......:   48.47  -14.73   40.04 -128.69   38.17  116.23 AMP/DG
 <816   > LOSS=   .538:    (   .254)       (   .145)       (   .139)    kW
 ---------------------*--------A-------*-------B-------*-------C-------*--------
 NODE: 816       VOLTS:   1.017   -2.26   1.025 -122.71   1.020  118.01 MAG/ANG
                   -LD:     .00     .00     .00     .00     .00     .00 kW/kVR
 kVll  24.900      CAP:             .00             .00             .00 kVR

 FROM NODE 850   .....:   48.47  -14.74   40.04 -128.70   38.17  116.23 AMP/DG
 <816   > LOSS=   .538:    (   .254)       (   .145)       (   .139)    kW
 TO NODE 818   .......:   13.02  -26.69                                  AMP/DG
 <818   > LOSS=   .154:    (   .154)                                     kW
 TO NODE 824   .......:   35.83  -10.42   40.04 -128.70   38.17  116.23 AMP/DG
 <824   > LOSS= 14.181:    (  4.312)       (  5.444)       (  4.425)    kW
```

```
- R A D I A L   P O W E R   F L O W  ---  DATE:  6-24-2004 AT 16:34:32 HOURS ---
 SUBSTATION:  IEEE 34;   FEEDER:  IEEE 34
 ------------------------------------------------------------------------------
    NODE      VALUE         PHASE A         PHASE B         PHASE C     UNT O/L<
                            (LINE A)        (LINE B)        (LINE C)        60.%
 ---------------------*--------A-------*-------B-------*-------C-------*--------
 NODE: 818       VOLTS:   1.016   -2.27                                  MAG/ANG
                   -LD:     .00     .00                                  kW/kVR
 kVll  24.900      CAP:              .00                                  kVR

 FROM NODE 816   .....:   13.03  -26.77                                  AMP/DG
 <818   > LOSS=   .154:    (   .154)                                     kW
 TO NODE 820   .......:   13.03  -26.77                                  AMP/DG
 <820   > LOSS=  3.614:    (  3.614)                                     kW
 ---------------------*--------A-------*-------B-------*-------C-------*--------
 NODE: 820       VOLTS:    .993   -2.32                                  MAG/ANG
                   -LD:     .00     .00                                  kW/kVR
 kVll  24.900      CAP:              .00                                  kVR

 FROM NODE 818   .....:   10.62  -28.98                                  AMP/DG
 <820   > LOSS=  3.614:    (  3.614)                                     kW
 TO NODE 822   .......:   10.62  -28.98                                  AMP/DG
 <822   > LOSS=   .413:    (   .413)                                     kW
 ---------------------*--------A-------*-------B-------*-------C-------*--------
 NODE: 822       VOLTS:    .990   -2.33                                  MAG/ANG
                   -LD:     .00     .00                                  kW/kVR
 kVll  24.900      CAP:              .00                                  kVR

 FROM NODE 820   .....:     .00     .00                                  AMP/DG
 <822   > LOSS=   .413:    (   .413)                                     kW
 ---------------------*--------A-------*-------B-------*-------C-------*--------
 NODE: 824       VOLTS:   1.008   -2.37   1.016 -122.94   1.012  117.76 MAG/ANG
                   -LD:     .00     .00     .00     .00     .00     .00 kW/kVR
 kVll  24.900      CAP:              .00             .00             .00 kVR

 FROM NODE 816   .....:   35.87  -10.70   39.82 -129.02   38.05  116.25 AMP/DG
 <824   > LOSS= 14.181:    (  4.312)       (  5.444)       (  4.425)     kW
 TO NODE 826   .......:                    3.10 -148.92                  AMP/DG
 <826   > LOSS=   .008:                    (   .008)                     kW
 TO NODE 828   .......:   35.87  -10.70   36.93 -127.39   38.05  116.25 AMP/DG
 <828   > LOSS=  1.108:    (   .361)       (   .393)       (   .354)     kW
 ---------------------*--------A-------*-------B-------*-------C-------*--------
 NODE: 826       VOLTS:                   1.016 -122.94                  MAG/ANG
                   -LD:                     .00     .00                  kW/kVR
 kVll  24.900      CAP:                             .00                  kVR

 FROM NODE 824   .....:                     .00     .00                  AMP/DG
 <826   > LOSS=   .008:                    (   .008)                     kW
```

```
- R A D I A L  P O W E R  F L O W  ---  DATE:  6-24-2004 AT 16:34:32 HOURS ---
 SUBSTATION:  IEEE 34;   FEEDER:  IEEE 34
 ------------------------------------------------------------------------------
    NODE      VALUE         PHASE A         PHASE B         PHASE C     UNT O/L<
                            (LINE A)        (LINE B)        (LINE C)        60.%
 ---------------------*--------A-------*-------B-------*-------C-------*--------
 NODE: 828       VOLTS:   1.007   -2.38   1.015 -122.95   1.011  117.75 MAG/ANG
                   -LD:     .00     .00     .00     .00     .00     .00 kW/kVR
 kVll  24.900      CAP:             .00             .00             .00 kVR

 FROM NODE 824   .....:   35.87  -10.72   36.93 -127.41   37.77  116.42 AMP/DG
 <828   > LOSS=  1.108:    (   .361)       (   .393)       (   .354)    kW
 TO NODE 830   .......:   35.87  -10.72   36.93 -127.41   37.77  116.42 AMP/DG
 <830   > LOSS= 26.587:    (  8.443)       (  9.214)       (  8.930)    kW
 ---------------------*--------A-------*-------B-------*-------C-------*--------
 NODE: 830       VOLTS:    .989   -2.63    .998 -123.39    .994  117.25 MAG/ANG
                  D-LD:    9.95    4.98    9.86    4.93   24.55    9.82 kW/kVR
 kVll  24.900    Y CAP:             .00             .00             .00 kVR

 FROM NODE 828   .....:   35.43  -11.06   36.91 -127.92   37.79  115.96 AMP/DG
 <830   > LOSS= 26.587:    (  8.443)       (  9.214)       (  8.930)    kW
 TO NODE 854   .......:   34.22   -9.97   36.19 -127.47   36.49  116.26 AMP/DG
 <854   > LOSS=   .635:    (   .197)       (   .227)       (   .211)    kW
 ---------------------*--------A-------*-------B-------*-------C-------*--------
 NODE: 854       VOLTS:    .989   -2.64    .998 -123.40    .993  117.24 MAG/ANG
                   -LD:     .00     .00     .00     .00     .00     .00 kW/kVR
 kVll  24.900      CAP:             .00             .00             .00 kVR

 FROM NODE 830   .....:   34.23   -9.99   36.19 -127.48   36.49  116.25 AMP/DG
 <854   > LOSS=   .635:    (   .197)       (   .227)       (   .211)    kW
 TO NODE 852   .......:   34.23   -9.99   35.93 -127.72   36.49  116.25 AMP/DG
 <852   > LOSS= 44.798:    ( 13.996)       ( 15.778)       ( 15.023)    kW
 TO NODE 856   .......:                     .31  -98.70                 AMP/DG
 <856   > LOSS=   .001:                    (   .001)                   kW
 ---------------------*--------A-------*-------B-------*-------C-------*--------
 NODE: 852       VOLTS:    .958   -3.11    .968 -124.18    .964  116.33 MAG/ANG
                   -LD:     .00     .00     .00     .00     .00     .00 kW/kVR
 kVll  24.900      CAP:             .00             .00             .00 kVR

 FROM NODE 854   .....:   34.35  -11.00   35.90 -128.66   36.52  115.41 AMP/DG
 <852   > LOSS= 44.798:    ( 13.996)       ( 15.778)       ( 15.023)    kW
 TO NODE RG11  .<VRG>.:   34.35  -11.00   35.90 -128.66   36.52  115.41 AMP/DG
 <RG11  > LOSS=   .000:    (   .000)       (   .000)       (   .000)    kW
 ---------------------*--------A-------*-------B-------*-------C-------*--------
 NODE: RG11      VOLTS:   1.036   -3.11   1.035 -124.18   1.036  116.33 MAG/ANG
                   -LD:     .00     .00     .00     .00     .00     .00 kW/kVR
 kVll  24.900      CAP:             .00             .00             .00 kVR

 FROM NODE 852   <VRG>:   31.77  -11.00   33.59 -128.66   33.98  115.41 AMP/DG
 <RG11  > LOSS=   .000:    (   .000)       (   .000)       (   .000)    kW
 TO NODE 832   .......:   31.77  -11.00   33.59 -128.66   33.98  115.41 AMP/DG
 <832   > LOSS=   .011:    (   .003)       (   .004)       (   .004)    kW
```

```
- R A D I A L   P O W E R   F L O W  ---  DATE:  6-24-2004 AT 16:34:32 HOURS ---
 SUBSTATION:  IEEE 34;   FEEDER:  IEEE 34
 ------------------------------------------------------------------------------
    NODE      VALUE         PHASE A         PHASE B         PHASE C     UNT O/L<
                            (LINE A)        (LINE B)        (LINE C)        60.%
 ---------------------*--------A-------*-------B-------*-------C-------*--------
 NODE: 832       VOLTS:   1.036   -3.11   1.035 -124.18   1.036  116.33 MAG/ANG
                   -LD:     .00     .00     .00     .00     .00     .00 kW/kVR
 kVll  24.900      CAP:             .00             .00             .00 kVR

 FROM NODE RG11  .....:   31.77  -11.00   33.59 -128.66   33.98  115.41 AMP/DG
 <832   > LOSS=   .011:    (   .003)       (   .004)       (   .004)    kW
 TO NODE 858   .......:   21.31     .47   23.40 -116.89   24.34  128.36 AMP/DG
 <858   > LOSS=  2.467:    (   .643)       (   .997)       (   .827)    kW
 TO NODE XF10  .......:   11.68  -32.29   11.70 -152.73   11.61   87.39 AMP/DG <
 <XF10  > LOSS=  9.625:    (  3.196)       (  3.241)       (  3.187)    kW
 ---------------------*--------A-------*-------B-------*-------C-------*--------
 NODE: 858       VOLTS:   1.034   -3.17   1.032 -124.28   1.034  116.22 MAG/ANG
                   -LD:     .00     .00     .00     .00     .00     .00 kW/kVR
 kVll  24.900      CAP:             .00             .00             .00 kVR

 FROM NODE 832   .....:   20.86     .86   23.13 -116.39   24.02  128.48 AMP/DG
 <858   > LOSS=  2.467:    (   .643)       (   .997)       (   .827)    kW
 TO NODE 834   .......:   20.73    1.01   23.13 -116.39   24.02  128.48 AMP/DG
 <834   > LOSS=  2.798:    (   .717)       (  1.145)       (   .936)    kW
 TO NODE 864   .......:     .14  -22.82                                  AMP/DG
 <864   > LOSS=   .000:    (   .000)                                    kW
 ---------------------*--------A-------*-------B-------*-------C-------*--------
 NODE: 834       VOLTS:   1.031   -3.24   1.029 -124.39   1.031  116.09 MAG/ANG
                   -LD:     .00     .00     .00     .00     .00     .00 kW/kVR
 kVll  24.900      CAP:             .00             .00             .00 kVR

 FROM NODE 858   .....:   20.29    2.18   22.37 -116.07   23.23  130.06 AMP/DG
 <834   > LOSS=  2.798:    (   .717)       (  1.145)       (   .936)    kW
 TO NODE 842   .......:   14.75   34.68   16.30  -95.63   15.12  151.05 AMP/DG
 <842   > LOSS=   .064:    (   .015)       (   .032)       (   .017)    kW
 TO NODE 860   .......:   11.16  -43.05    9.09 -154.82   10.60   99.34 AMP/DG
 <860   > LOSS=   .141:    (   .021)       (   .104)       (   .017)    kW
 ---------------------*--------A-------*-------B-------*-------C-------*--------
 NODE: 842       VOLTS:   1.031   -3.25   1.029 -124.39   1.031  116.09 MAG/ANG
                   -LD:     .00     .00     .00     .00     .00     .00 kW/kVR
 kVll  24.900      CAP:             .00             .00             .00 kVR

 FROM NODE 834   .....:   14.74   34.67   16.30  -95.64   15.12  151.03 AMP/DG
 <842   > LOSS=   .064:    (   .015)       (   .032)       (   .017)    kW
 TO NODE 844   .......:   14.74   34.67   16.30  -95.64   15.12  151.03 AMP/DG
 <844   > LOSS=   .306:    (   .068)       (   .156)       (   .083)    kW
```

```
- R A D I A L   P O W E R   F L O W  ---  DATE:  6-24-2004 AT 16:34:32 HOURS ---
 SUBSTATION:  IEEE 34;   FEEDER:  IEEE 34
 ------------------------------------------------------------------------------
    NODE      VALUE         PHASE A         PHASE B         PHASE C     UNT O/L<
                            (LINE A)        (LINE B)        (LINE C)        60.%
 ---------------------*--------A-------*-------B-------*-------C-------*--------
 NODE: 844       VOLTS:   1.031   -3.27   1.029 -124.42   1.031  116.06 MAG/ANG
                  Y-LD:  143.41  111.54  142.97  111.20  143.51  111.62 kW/kVR
 kVll  24.900    Y CAP:          106.23          105.90          106.31 kVR

 FROM NODE 842   .....:   14.47   37.12   16.29  -95.71   15.11  150.97 AMP/DG
 <844   > LOSS=   .306:    (   .068)       (   .156)       (   .083)    kW
 TO NODE 846   .......:    9.83   78.88    9.40  -63.87    9.40 -170.67 AMP/DG
 <846   > LOSS=   .323:    (   .043)       (   .212)       (   .068)    kW
 ---------------------*--------A-------*-------B-------*-------C-------*--------
 NODE: 846       VOLTS:   1.031   -3.32   1.029 -124.46   1.031  116.01 MAG/ANG
                   -LD:     .00     .00     .00     .00     .00     .00 kW/kVR
 kVll  24.900      CAP:             .00             .00             .00 kVR

 FROM NODE 844   .....:    9.76   78.80    9.40  -52.54    9.78 -161.93 AMP/DG
 <846   > LOSS=   .323:    (   .043)       (   .212)       (   .068)    kW
 TO NODE 848   .......:    9.76   78.80    9.40  -52.54    9.78 -161.93 AMP/DG
 <848   > LOSS=   .048:    (   .007)       (   .031)       (   .010)    kW
 ---------------------*--------A-------*-------B-------*-------C-------*--------
 NODE: 848       VOLTS:   1.031   -3.32   1.029 -124.47   1.031  116.00 MAG/ANG
                  D-LD:   20.00   16.00   20.00   16.00   20.00   16.00 kW/kVR
 kVll  24.900    Y CAP:          159.43          158.86          159.56 kVR

 FROM NODE 846   .....:    9.76   78.79    9.77  -42.47    9.78 -161.94 AMP/DG
 <848   > LOSS=   .048:    (   .007)       (   .031)       (   .010)    kW
 ---------------------*--------A-------*-------B-------*-------C-------*--------
 NODE: 860       VOLTS:   1.030   -3.24   1.029 -124.39   1.031  116.09 MAG/ANG
                  Y-LD:   20.00   16.00   20.00   16.00   20.00   16.00 kW/kVR
 kVll  24.900    Y CAP:             .00             .00             .00 kVR

 FROM NODE 834   .....:    5.87  -33.62    7.68 -156.52    5.29   86.10 AMP/DG
 <860   > LOSS=   .141:    (   .021)       (   .104)       (   .017)    kW
 TO NODE 836   .......:    4.16  -30.19    5.96 -154.63    3.60   90.25 AMP/DG
 <836   > LOSS=   .039:    (  -.035)       (   .103)       (  -.028)    kW
 ---------------------*--------A-------*-------B-------*-------C-------*--------
 NODE: 836       VOLTS:   1.030   -3.23   1.029 -124.39   1.031  116.09 MAG/ANG
                   -LD:     .00     .00     .00     .00     .00     .00 kW/kVR
 kVll  24.900      CAP:             .00             .00             .00 kVR

 FROM NODE 860   .....:    1.49  -19.83    4.42 -150.74    1.74   68.08 AMP/DG
 <836   > LOSS=   .039:    (  -.035)       (   .103)       (  -.028)    kW
 TO NODE 840   .......:    1.50  -20.01    2.33 -151.97    1.75   68.00 AMP/DG
 <840   > LOSS=   .002:    (  -.014)       (   .026)       (  -.010)    kW
 TO NODE 862   .......:     .00     .00    2.09 -149.38     .00     .00 AMP/DG
 <862   > LOSS=   .000:    (  -.005)       (   .009)       (  -.004)    kW
```

```
- R A D I A L   P O W E R   F L O W  ---  DATE:  6-24-2004 AT 16:34:32 HOURS ---
 SUBSTATION:  IEEE 34;   FEEDER:  IEEE 34
 ------------------------------------------------------------------------------
    NODE      VALUE         PHASE A         PHASE B         PHASE C     UNT O/L<
                            (LINE A)        (LINE B)        (LINE C)        60.%
 ---------------------*--------A-------*-------B-------*-------C-------*--------
 NODE: 840       VOLTS:   1.030   -3.23   1.029 -124.39   1.031  116.09 MAG/ANG
                  Y-LD:    9.27    7.21    9.26    7.20    9.28    7.22 kW/kVR
 kVll  24.900    Y CAP:             .00             .00             .00 kVR

 FROM NODE 836   .....:     .79  -41.11     .79 -162.26     .79   78.21 AMP/DG
 <840   > LOSS=   .002:    ( -.014)       (  .026)       ( -.010)     kW
 ---------------------*--------A-------*-------B-------*-------C-------*--------
 NODE: 862       VOLTS:   1.030   -3.23   1.029 -124.39   1.031  116.09 MAG/ANG
                   -LD:     .00     .00     .00     .00     .00     .00 kW/kVR
 kVll  24.900      CAP:             .00             .00             .00 kVR

 FROM NODE 836   .....:     .00     .00    2.09 -149.50     .00     .00 AMP/DG
 <862   > LOSS=   .000:    ( -.005)       (  .009)       ( -.004)     kW
 TO NODE 838   ........:                   2.09 -149.50                 AMP/DG
 <838   > LOSS=   .004:                   (  .004)                     kW
 ---------------------*--------A-------*-------B-------*-------C-------*--------
 NODE: 838       VOLTS:                  1.029 -124.39                 MAG/ANG
                   -LD:                    .00     .00                 kW/kVR
 kVll  24.900      CAP:                            .00                 kVR

 FROM NODE 862   .....:                    .00     .00                 AMP/DG
 <838   > LOSS=   .004:                   (  .004)                     kW
 ---------------------*--------A-------*-------B-------*-------C-------*--------
 NODE: 864       VOLTS:   1.034   -3.17                                 MAG/ANG
                   -LD:     .00     .00                                 kW/kVR
 kVll  24.900      CAP:             .00                                 kVR

 FROM NODE 858   .....:     .00     .00                                 AMP/DG
 <864   > LOSS=   .000:    (  .000)                                     kW
 ---------------------*--------A-------*-------B-------*-------C-------*--------
 NODE: XF10      VOLTS:   1.000   -4.63    .998 -125.73   1.000  114.82 MAG/ANG
                   -LD:     .00     .00     .00     .00     .00     .00 kW/kVR
 kVll   4.160      CAP:             .00             .00             .00 kVR

 FROM NODE 832   .....:   69.90  -32.29   70.04 -152.73   69.50   87.39 AMP/DG <
 <XF10  > LOSS=  9.625:    ( 3.196)       ( 3.241)       ( 3.187)     kW
 TO NODE 888   ........:   69.90  -32.29   70.04 -152.73   69.50   87.39 AMP/DG
 <888   > LOSS=   .000:    (  .000)       (  .000)       (  .000)     kW
 ---------------------*--------A-------*-------B-------*-------C-------*--------
 NODE: 888       VOLTS:   1.000   -4.64    .998 -125.73   1.000  114.82 MAG/ANG
                   -LD:     .00     .00     .00     .00     .00     .00 kW/kVR
 kVll   4.160      CAP:             .00             .00             .00 kVR

 FROM NODE XF10  .....:   69.90  -32.29   70.04 -152.73   69.50   87.39 AMP/DG
 <888   > LOSS=   .000:    (  .000)       (  .000)       (  .000)     kW
 TO NODE 890   ........:   69.90  -32.29   70.04 -152.73   69.50   87.39 AMP/DG
 <890   > LOSS= 32.760:    ( 11.638)      (  9.950)      ( 11.173)     kW
```

```
- R A D I A L  P O W E R  F L O W  ---  DATE:  6-24-2004 AT 16:34:32 HOURS ---
 SUBSTATION:  IEEE 34;   FEEDER:  IEEE 34
 ------------------------------------------------------------------------------
    NODE      VALUE          PHASE A          PHASE B          PHASE C     UNT O/L<
                             (LINE A)         (LINE B)         (LINE C)         60.%
 ---------------------*--------A-------*-------B-------*-------C--------*---------
 NODE: 890       VOLTS:    .917   -5.19    .924 -126.78    .918  113.98 MAG/ANG
                  D-LD:  139.11   69.55  137.56   68.78  137.01   68.50 kW/kVR
 kVll   4.160    Y CAP:             .00             .00             .00 kVR

 FROM NODE 888   .....:   69.91  -32.31   70.05 -152.75   69.51   87.37 AMP/DG
 <890   > LOSS= 32.760:    ( 11.638)       (  9.950)       ( 11.173)    kW
 ---------------------*--------A-------*-------B-------*-------C--------*---------
 NODE: 856       VOLTS:                    .998 -123.41                  MAG/ANG
                   -LD:                     .00     .00                  kW/kVR
 kVll  24.900      CAP:                             .00                  kVR

 FROM NODE 854   .....:                     .00     .00                  AMP/DG
 <856   > LOSS=   .001:                   (   .001)                     kW
```